Aus dem Institut für Anatomie

der Medizinischen Fakultät Charité – Universitätsmedizin Berlin

DISSERTATION

Kinase pathways involved in the vasopressin signaling along the distal nephron: roles of SPAK and OSR1 kinases

zur Erlangung des akademischen Grades

Doctor medicinae (Dr. med.)

vorgelegt der Medizinischen Fakultät

Charité – Universitätsmedizin Berlin

von

Turgay Saritas

aus Hattingen

Datum der Promotion: 14.02.2014

Zusammenfassung

Der Na^+-K^+-$2Cl^-$-Kotransporter (NKCC2) im dicken aufsteigenden Teil der Henle-Schleife (TAL) und der Na^+-Cl^-- Kotransporter (NCC) im distalen Konvolut (DCT) sind entscheidend an der Regulation der renalen Salzausscheidung beteiligt. Somit spielen die beiden Transporter eine wichtige Rolle bei der Aufrechterhaltung des extrazellulären Volumens und des Blutdrucks. Die Aktivität der Transporter wird durch Trafficking und Phosphorylierung bestimmt. Diese Vorgänge können endokrin moduliert werden. Es war bekannt, dass das antidiuretische Hormon (ADH, Vasopressin) neben seiner Wirkung auf den Wassertransport im Sammelrohr auch den distalen Salztransport über seinen V2 Rezeptor stimulieren kann. *With-no-lysin [K]*-Kinasen (WNK) waren als Teil des Signalwegs zu Transportern identifiziert. Ihre katalytische Wirkung aktiviert weitere Kinasen, zu denen die homologen, Ste20-ähnlichen SPAK und OSR1 rechnen. Vorarbeiten zeigten, dass diese wiederum die zwei Kotransporter an ihren N-terminalen Threonin- bzw. Serinresten phosphorylieren und somit aktivieren können. Ziel der vorliegenden Arbeit waren die segmentspezifische Charakterisierung der beiden Kinasen und ihre Rolle bei der Vermittlung ADH-induzierter Stimuli jeweils in TAL und DCT. Mithilfe von SPAK-/- Mäusen konnten wir zeigen, dass trotz der Koexpression von SPAK und OSR1 entlang dem distalen Nephron segmentspezifische, nicht-redundante Rollen von OSR1 und SPAK für die Regulation von NKCC2 bzw. NCC identifizierbar waren; die NKCC2-Phosphorylierung war hier stark erhöht, die von NCC jedoch deutlich reduziert. In einem kooperativen Ansatz konnten wir diesen verwirrenden Phänotyp aufklären. Eine nierenspezifische SPAK-Spleißvariante mit trunzierter Kinase-Domäne und dominant-negativen Eigenschaften (*kidney-specific* [KS]-SPAK) wurde identifiziert. In Kontrollen war KS-SPAK funktionell hauptsächlich im TAL belegbar und hemmte hier kompetitiv OSR1 sowie die aktive *full-length* SPAK Form (FL-SPAK); KS-SPAK bewirkt hierdurch offenbar auch eine Deaktivierung von NKCC2. Im Gegensatz dazu war die Aktivierung von NCC kritisch von der reichlich im DCT exprimierten FL-SPAK abhängig. ADH-defiziente Brattleboro-Ratten mit zentralem Diabetes Insipidus (DI) wurden als Modell für extrinsische ADH-Stimulation eingesetzt. Akute ADH-Gabe stimulierte sowohl NKCC2 wie auch NCC durch deren gesteigerte Oberflächenexpression und Phosphorylierung. Im DCT wurde FL-SPAK hierbei als Schlüsselkomponente der ADH-Signaltransduktion identifiziert; dies betraf sowohl die akuten als auch die chronischen Effekte des Hormons. Im TAL waren SPAK und OSR1 unter ADH gleichermaßen

aktiviert, zusätzlich war die inhibitorische KS-SPAK quantitativ reduziert. Die Ergebnisse der vorliegenden Arbeit zeigen neue Aspekte der Funktion des WNK-SPAK/OSR1-NKCC2/NCC Signalnetzwerks im distalen Nephron und charakterisieren die Phosphokinase SPAK neben OSR1 als ein wichtiges Zwischenglied der ADH-induzierten Transportaktivierung. Die vorgestellten Daten liefern neue Aspekte zur Physiologie der Harnkonzentrierung und zur Regulation der NaCl-Ausscheidung. In der Perspektive rücken die Kinasen SPAK und OSR1 in den Vordergrund therapeutischer Beeinflussungsmöglichkeiten von Wasser- und Elektrolythomöostase.

Schlüsselwörter: dicker aufsteigenden Teil der Henle-Schleife, distaler Tubulus, NCC, NKCC2, SPAK, OSR1, Vasopressin, AVP

Abstract

The Na^+-K^+-$2Cl^-$-cotransporter (NKCC2) of thick ascending limb (TAL) and the Na^+-Cl^--cotransporter (NCC) of distal convoluted tubule (DCT) are critical for renal salt handling. The two cotransporters have an important role in maintaining extracellular volume and blood pressure. Principally, activity of the two closely related transporters is determined by their luminal trafficking and phosphorylation. These processes can be modulated by endocrine stimuli. Recent studies have clarified V2-receptor mediated effects of vasopressin (AVP; antidiuretic hormone) in the distal nephron, leading to increased salt reabsorption along with the stimulation of water transport in the collecting duct. With-no-lysine [K]) kinases (WNK) have been recognized as a part of this signaling pathway. The catalytic effects of WNKs are typically mediated by other downstream kinases, among which the two homologous Ste20-like kinases SPAK and OSR1 are important because of their ability to directly phosphorylate NKCC2 and NCC at their conserved N-terminal threonine- and serine residues. This work was aimed at a segment-specific elucidation of the roles of SPAK and OSR1 in mediating the effects of AVP in TAL and DCT. SPAK-deletion in mice was associated with increased NKCC2 but decreased NCC phosphorylation, indicating a segment-specific role of the kinase in the regulation of these transporters. OSR1, although largely co-expressed with SPAK, failed to compensate for SPAK deficiency, suggesting non-redundant roles for the two kinases. A novel, kidney-specific SPAK splice variant (KS-SPAK) with a truncated kinase-domain and dominant-negative properties was identified. In controls, KS-SPAK was predominantly distributed in TAL, where it inhibited OSR1 and full-length SPAK (FL-SPAK) in a competitive manner. KS-SPAK hereby caused the deactivation of NKCC2. In contrast, FL-SPAK was predominantly expressed in DCT, providing NCC phosphorylation. AVP-deficient Brattleboro-rats with central diabetes insipidus were used as models for extrinsic AVP-stimulation. Acute AVP-administration stimulated NKCC2 and NCC by increasing its trafficking and phosphorylation. In DCT, FL-SPAK was identified as a key component of AVP-signaling; this refers to acute and chronic effects of this hormone as well. In TAL, SPAK and OSR1 were both involved in mediating the effects of AVP. Additionally, expression of KS-SPAK was reduced upon AVP. These data have revealed new aspects of the WNK-SPAK/OSR1-NKCC2/NCC cascade, characterizing SPAK and OSR1 as the major kinases in AVP-induced activation of the distal salt transporters. Data extend information on the physiology of

urine concentration and the regulation of salt excretion. SPAK and OSR1 will thus be a potential focus for targets to targeting water- and electrolyte homeostasis.

Key words: thick ascending limb of henle's loop, distale tubulus, NCC, NKCC2, SPAK, OSR1, Vasopressin, AVP.

ABBREVIATIONS

ADH	antidiuretic hormone, also known as AVP
AMPK	AMP activated kinase
Ang II	Angiotensin II
ANP	atrial natriuretic peptide
AP3	adapter protein 3
AQP	aquaporin
AVP	arginine vasopressin
BSA	bovine serum albumin
C	cortical
cAMP	cyclic adenosine monophosphate
CCC	cation-coupled chloride cotransporter
CD	collecting ducts
CDI	central diabetes insipidus
cGMP	cyclic guanosine monophosphate
Cl^-	chloride
CNT	connecting tubules
C-terminal	carboxyl-terminal, COOH-terminal
Cy	cyanine
DAPI	4', 6-diamidino-2-phenylindole
DCT	distal convoluted tubule
DCT2	late part of distal convoluted tubule

dDAVP	desmopressin, deamino-Cys^{1},D-Arg^{8} vasopressin
DI rats	Brattleboro rats with central diabetes insipidus
ECF	extracellular fluid
e.g.	for example
EM	electron microscopy
ENaC	epithelial sodium channel
ER	endoplasmic reticulum
FE	fractional excretion
Fig	figure
FHHt	familial hyperkalemic hypertension, also known as Gordon's syndrome
FL-SPAK	full-length-SPS-related proline/alanine-rich kinase
GCK	germinal center kinase
GPI	glycosylphosphatidylinositol
HRP	horseradish peroxidase
IgG	immunoglobulin G
IP	immunoprecipitation
K^+	potassium
kDa	kilo dalton
KS	kidney-specific
M	medullary
MAPK	mitogen-activated protein kinase
MD	macula densa

mosm/kg H20	milliosmol per kilogram water
Na^+	sodium
Na-Pi	sodium-phosphate cotransporter
NCC	sodium-chloride-cotransporter
NDI	nephrogenic diabetes insipidus
NHE	sodium-hydrogen exchanger
NKCC2	sodium-potassium-chloride-cotransporter type 2
nm	nanometer
NO	nitric oxide
N-terminal	amino-terminal, NHE2-terminal
OM	outer medullary
OSR1	oxidative stress response kinase-1
P	phosphorylation
PAPA	proline-alanine repeating sequence
PBS	phosphate buffered saline
PCR	polymerase chain reaction
PDE2	phosphodiesterase 2
PFA	paraformaldehyde
PHAII	pseudohypoaldosteronism type II
PKA	protein kinase A
PM	plasma membrane
PT	proximal tubule

PTH	parathyroid hormone
RAAS	renin-angiotensin-aldosterone system
Ref.	references
REGM	renal epithelial cell growth medium
ROMK	rat outer medullary potassium channel
RT-PCR	reverse transcription polymerase chain reaction
S	serine
SD	standard deviation
SDS-PAGE	sodium dodecyl sulfate polyacrylamide gel electrophoresis
SEM	standard error of the mean
SGLT	sodium-dependent glucose cotransporter
SIADH	syndrome of inappropriate secretion of antidiuretic hormone
SLC	solute carrier family
SNP	single nucleotide polymorphism
Sort	sortilin
SPAK	SPS-related proline/alanine-rich kinase
SPAK2	alternativly translated sterile 20/SPS1-related proline/alanine-rich kinase
SPAK-/-	SPS-related proline/alanine-rich kinase knockout mice
T	threonine
TAL	thick ascending limp of henle's loop
TGN	trans-golgi network
THP	Tamm-Horsfall protein

V1R	vasopressin type 1 receptor
V2R	vasopressin type 2 receptor
VAMP	vesicle-associated membrane proteins
vs.	versus
WNK	with no lysine K kinase
WT	wild type

TABLE OF CONTENTS

LIST OF FIGURES

Present results have been obtained by my own experimental work unless indicated here:

Figure 4: by courtesy of Dr. K. Mutig, Institute for Anatomy, Charité Universitätsmedizin Berlin.

Figure 8 C, D: immunogold staining was performed by our technical assistants.

Figure 12: by courtesy of Dr. T. Kahl, Institute for Anatomy, Charité Universitätsmedizin Berlin.

Figure 16 A: by courtesy of James A. McCormick, OHSU, Portland, OR.

Figure 22 A-H: immunogold staining was performed by our technical assistants.

Figure 26 A-B: Co-IP was performed by C. Dathe, Institute for Anatomy, Charité Universitätsmedizin Berlin.

Figure 27: results were obtained by A. Terker, OHSU, Portland, OR.

1. Introduction

1.1. Renal cation chloride cotransporters and arterial pressure

High blood pressure (hypertension) is the most important preventable risk factor of death worldwide (1). According to the WHO data, 40% of adults aged 25 and over suffer from high blood pressure which causes 7.5 million deaths per year (2). Arterial pressure is the product of peripheral resistance to blood flow and the circulating blood volume. The sodium cation (Na^+) is the main plasma osmolyte and the key determinant of extracellular fluid volume and blood pressure. A high intake of salt (NaCl or sodium chloride, the main ingredient in edible salt) is an important risk factor for hypertension. The correlation between salt-intake and blood pressure is obvious in populations consuming extremely little (<3g/day) or extremely much salt (>20g/day) (3). Interestingly, blood pressure reduction in response to dietary sodium restriction is more pronounced in hypertensive compared to normotensive individuals. Overall, daily reduction of salt intake by 5 g could relieve the severity of hypertension in many cases and prevent about 3 million deaths from cardiovascular diseases per year worldwide (4). However, weak compliance of patients to low salt diet often leads to a situation where the pharmacological management of hypertension becomes indispensable. Modern therapeutic strategies for lowering the blood pressure combine drugs with different mechanisms of action. The kidneys regulate the long-term blood volume by balancing urinary sodium and water excretion to dietary intake (5). Consequently, diuretics causing salt wasting due to their ability to inhibit the electroneutral cation-coupled chloride cotransporters (CCC) in the kidney (6) are considered as agents of the first line antihypertensive therapy. The renal members of CCC family include the Na^+-K^+-$2Cl^-$ cotransporter (NKCC2) and the Na^+-Cl^- cotransporter (NCC) which are targets for the diuretics furosemide and thiazides, respectively (7). Physiologically, NKCC2 and NCC mediate the reabsorption of sodium across epithelial cells of the distal nephron from urine to blood plasma. (8). Their significance for the maintenance of blood pressure is reflected by the therapeutic use of furosemide and thiazide diuretics. Two rare human genetic syndromes caused by loss-of-function mutations in the genes encoding NKCC2 or NCC, known as Bartter's type I syndrome and Gitelman's syndrome, respectively, further illustrate their impact. Both syndromes are characterized by impaired sodium-chloride reabsorption, hypotension, hypokalaemia, and metabolic alkalosis (9, 10). In

contrast, excessive NKCC2 or NCC activity may cause or significantly contribute to the pathogenesis of inherited and acquired forms of hypertension in humans and rodent models (11-14).

1.2. The segment-specific roles of NKCC2 and NCC

The kidneys maintain nearly constant plasma osmolality and sodium concentration by regulating water and sodium excretion. The ability of the kidney to concentrate the urine is essential for survival of non-aquatic species, including humans. This function is executed by the balanced performance of nephrons and kidney vasculature (15, 16). Each human kidney has approximately one million nephrons. Nephron is the functional unit of the kidney and is composed of a glomerulus and its tubule system. The glomeruli filter the blood into the renal tubules lined by a single layer of epithelial cells and surrounded by blood capillaries (17). Apart from supplying the renal tubule with oxygen and nutrition, these anatomical relationships enable an effective reabsorption of water and solutes from the renal tubule back to the blood and a selective secretion of toxic substances into the tubule lumen (15, 16). The transcellular reabsorption of Na^+ is driven by the activity of the basolateral Na^+/K^+-ATPase and mediated by diverse sodium transporters and channels located in the luminal membrane of kidney epithelial cells (18). Two thirds of filtered Na^+ is reabsorbed in the proximal tubule chiefly via the sodium-hydrogen exchanger (NHE), the sodium-phosphate cotransporter (Na-Pi), and the sodium-dependent glucose cotransporter (SGLT) (Fig. 1), and a large volume of water follows via osmosis, resulting in an isotonic ion concentration at the beginning of the following Henle's Loop (19). The U-shaped Loop of Henle consists of a descending and ascending limb and is an important element of urinary concentration. After reaching the maximal osmolality of the filtrate in the loop bend, Na^+ can be reabsorbed in water-impermeable ascending limb by concentration gradient (16, 17). The following thick ascending limb of Henle's loop (TAL) reabsorbs 20-25% of Na^+ mainly due to the activity of the luminal NKCC2. The TAL is water-impermeable which leads to a progressive dilution of the urine and creation of the longitudinal osmotic gradient along this tubule, while the medullary interstitium becomes hypertonic. This action is also known as the "single-effect" of the countercurrent multiplication system (16, 20, 21). In continuation of TAL, 5-7% of the filtrated sodium is reabsorbed through the NCC in the distal convoluted tubule (DCT) (6).

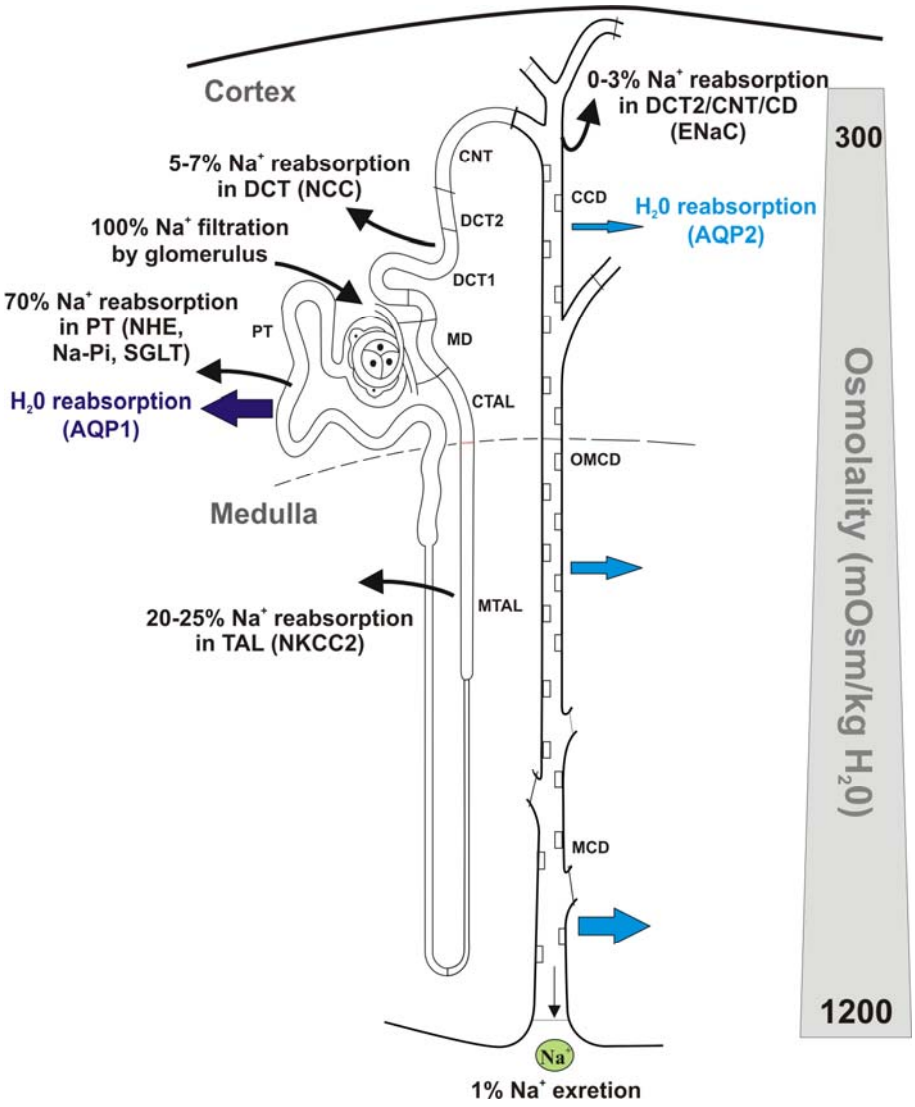

Figure 1: Sodium and water reabsorption in epithelial cells of kidney.

Simplified model of sodium and water reabsorption along the nephron segments. Sodium-chloride (NaCl) reabsorption by Na-H-exchanger (NHE), sodium-dependent glucose transporter (SGLT), Na^+-K^+-$2Cl^-$ type 2 cotransporter (NKCC2), Na^+-Cl^- cotransporter (NCC) and epithelial Na^+ channel (ENaC) and water reabsorption by Aquaporin 2 (AQP2) occur in distinct nephron segments indicated by arrows. Proximal tubule (PT), medullary (M) and cortical (C) thick ascending limb (TAL), macula densa (MD), distal convoluted tubule (DCT), connecting tubule (CNT) and cortical (C), outer medullary (OM) and medullary (M) collecting duct (CD) are shown. The cortical interstitium is nearly isotonic to plasma, while the inner medullary tip reaches an osmolality similar to that of urine during maximal urine concentration. The thickness of cyan arrows demonstrates the quantity of water reabsorption by AQP2.

Finally, in the last part of distal convoluted tubule (DCT2), connecting tubules (CNT) and collecting ducts (CD), approximately 3% of sodium reabsorption occurs chiefly through the amiloride-sensitive epithelial sodium channel (ENaC) (22). The final adjustment of salt reabsorption to balance the body sodium homeostasis occurs here (16).

Water reabsorption requires the presence of specialized water channels, aquaporins (AQP), and is largely dependent on the activity of renal NaCl transport systems. In PT, an isoosmotic reabsorption of 65-70% is accomplished via the constitutively expressed AQP1 (21), while the generation of the longitudinal osmotic gradient along the distal part of nephron due to NKCC2 activity is essential for the reabsorption of water in the collecting duct system through the inducible AQP2 and thus the production of concentrated urine (16).

The urinary concentrating mechanism is effectively governed by the endocrine system, mainly by the antidiuretic hormone (ADH), also known as vasopressin (AVP). Signalling via vasopressin type 2 receptor (V2R), AVP increases the activity of NKCC2 and triggers the incorporation of AQP2 water channels into the apical membrane of CD principal cells, leading to effective water reabsorption along the osmotic gradient and concentration of the urine up to 1,200 mOsm/kg H_2O in human (23-25).

1.3. Effects of AVP in the distal nephron

Generally, hormones can adjust blood pressure levels by affecting vascular smooth muscle contraction and/ or renal salt and water handling. Among other components of the major homeostatic control systems like the renin-angiotensin-aldosterone system (RAAS), the sympathetic nervous system, and atrial natriuretic peptide (ANP), AVP regulates both blood vessels and renal tubules (26). AVP is a pleiotropic nonapeptide, synthesized in the hypothalamus and secreted in the posterior pituitary gland in response to low blood pressure or high plasma osmolarity, usually indicating a water deficit (15, 16). At least three G- protein coupled vasopressin receptors exist in humans (27, 28). Vasopressin type 1a receptor (V1aR) is expressed in hepatocytes, platelets, brain, uterus and vascular smooth cells. In the latter, AVP favors vasoconstriction by increasing cellular calcium levels. V1aR is indirectly involved in the control of water and electrolyte transport in the kidney because of its downstream effects on blood pressure, glomerular filtration rate and vasa recta blood flow (27, 29). Vasopressin type 1b receptors (also known as V3) have been identified in the brain, in which they trigger temperature and memory control. Vasopressin type 2 receptor (V2R) is the best characterized of these receptors. The renal expression of V2R is limited to the distal nephron comprising TAL, DCT, CNT, and CD. Activation of the receptor triggers

intracellular cyclic adenosine monophosphate (cAMP) release which stimulates distinct signaling pathways to increase the function of relevant salt and water transport systems involved in urinary concentration (23, 30).

Impaired signal transduction along the AVP-V2R axis is associated with central (CDI) or nephrogenic diabetes insipidus (NDI), both leading to pronounced loss of water with the urine (31). In contrast, prolonged increase of blood AVP levels under certain pathological conditions results in excessive water retention with secondary hyponatriemia and is known as the syndrome of inappropriate secretion of antidiuretic hormone (SIADH) (32). Specific agonists and antagonists of AVP receptors were developed for the treatment of several AVP-related diseases and other disturbances of water balance, such as congestive heart failure with water retention and edema (33). Apart from its well known effects on water reabsorption, AVP significantly facilitates sodium and urea transport in the distal nephron and collecting duct to support the axial osmotic gradient required for efficient urine concentration (34, 35) (Fig. 2). The epithelial antidiuretic effects of the hormone are mediated by V2R abundantly expressed in TAL, DCT, and the principal cells of CNT and CD (36, 37).

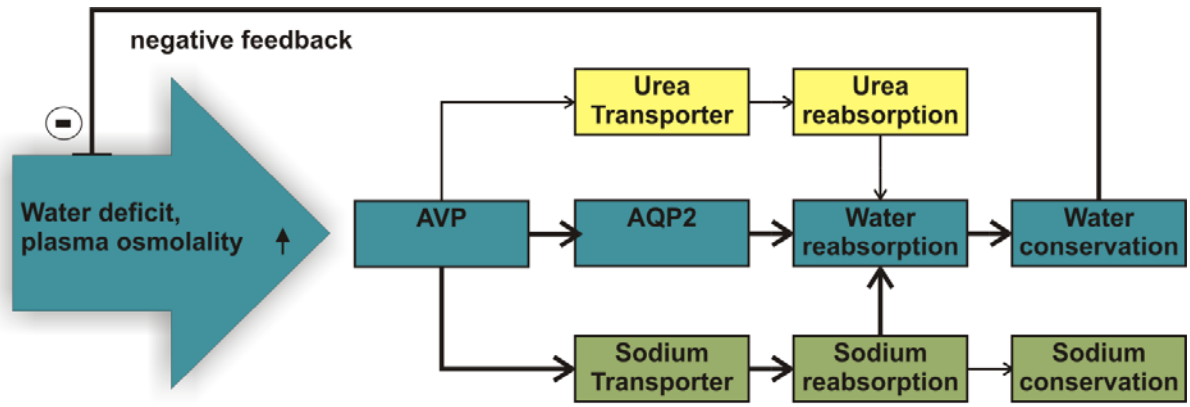

Figure 2: Renal effects of AVP.

Coordinate actions of AVP on sodium-, urea-, and water transport in the kidney. Salt conservation serves to maximize water resorption during urinary concentration. Adapted from ref. 38.

Previous studies have shown that the antidiuretic effect of AVP on water reabsorption requires less hormone concentration than the antinatriuretic effect within physiological limits of sodium reabsorption; the latter is active only when urine osmolarity reaches a certain threshold (27, 39). Physiological significance of V2R signaling in TAL has been established in a variety of experimental settings including short- and long-term

stimulation of mice and rats, microperfusion of isolated TAL tubules, as well as cell culture experiments with the V2R-agonist dDAVP (desmopressin, deamino-Cys[1],D-Arg[8] vasopressin) (40-42). These studies have identified NKCC2 as a major target of AVP. Activation of V2R in TAL was associated with increased surface expression, phosphorylation, and activity of the transporter (Fig. 3) (36, 43).

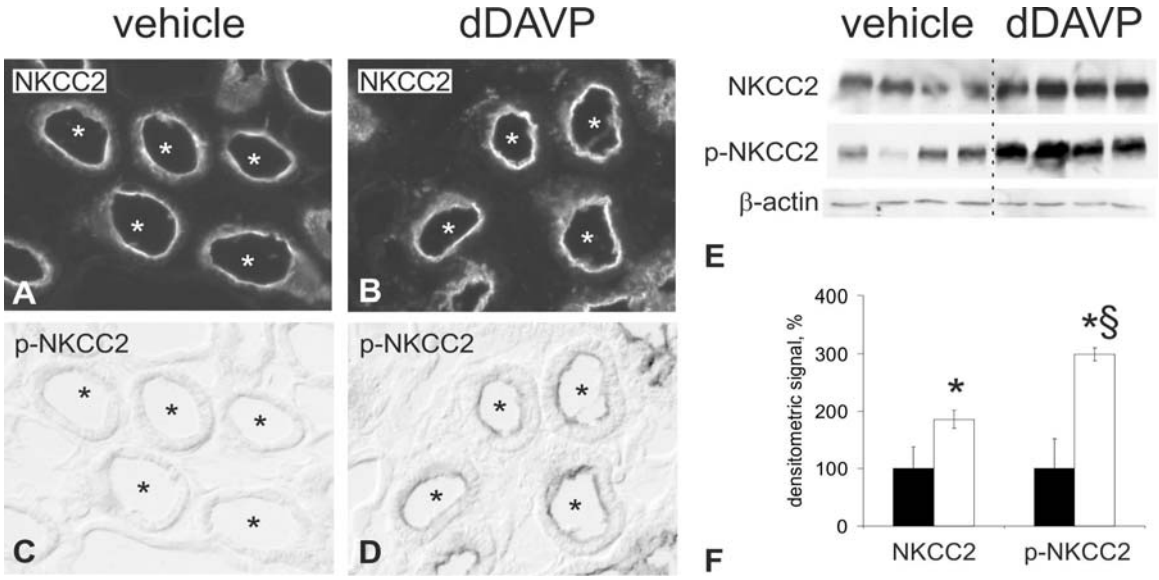

Figure 3: Effects of AVP on NKCC2 surface expression, phosphorylation and abundance

(A-D) Representative TAL profiles (asterisks) from vehicle- or dDAVP (desmopressin)-treated kidneys of Brattleboro rats with central diabetes insipidus (DI). Image pairs show NKCC2 and phospho (p)-NKCC2 immunostaining. Original magnification x400. (E) Western blot analysis of medullary kidney extracts from vehicle- and dDAVP-treated DI rats showing bands for NKCC2 and p-NKCC2 antibody at 160 kDa. β-actin- immunoreactive band serves as loading control (approximately 42 kDa). (F) Respective densitometric evaluations, with vehicle groups set at 100%. *P< 0.01 vs. vehicle. §P< 0.01, p-NKCC2 vs. NKCC2 in dDAVP group. Adapted from ref. 36.

In addition, significant AVP-induced increase of sodium reabsorption in the collecting duct due to stimulation of ENaC activity was described in several studies (38). This led to the hypothesis that AVP may contribute to development or aggravate certain forms of salt-sensitive hypertensive conditions (38, 44). However, despite the significant impact of NCC activity on the final urinary NaCl excretion, little information was available on effects of AVP in DCT. Significant expression of V2R in DCT has been established in a previous study utilizing in-situ hybridization for a high resolution analysis of V2R mRNA expression in the rat, mouse and human kidneys (Fig. 4) (36). Previous work has further demonstrated an increase in NCC abundance in Brattleboro rats with central diabetes insipidus (DI) when dDAVP had been chronically substituted, suggesting AVP-sensitivity within DCT (32). However it had remained unclear whether AVP acts directly within the DCT or whether it modulates the RAAS or other endocrine or paracrine pathways

systemically (27). Specific information on AVP-signaling in DCT was thus scarce (24, 27).

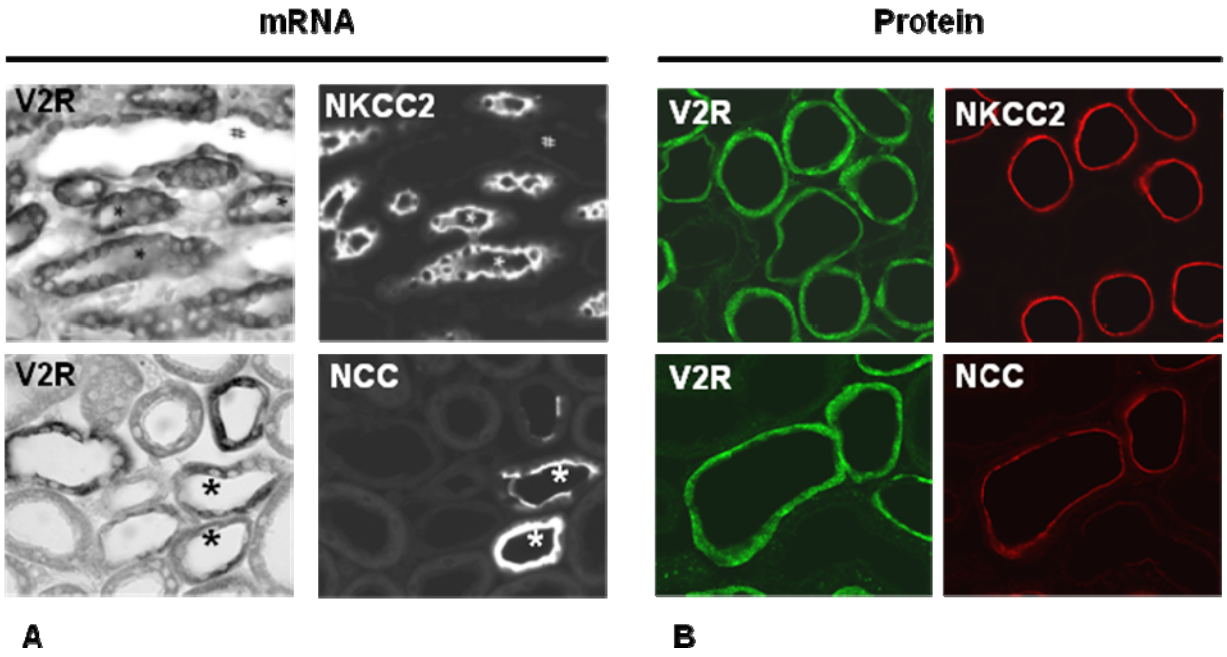

Figure 4: V2R mRNA and protein distribution in mTAL and DCT of Wistar rats.

(A) Labeling in consecutive serial sections demonstrates V2R mRNA distribution in mTAL (identified by NKCC2 immunostaining) and DCT (identified by NCC immunostaining). (B) Double-labeling of immunoreactive V2R and NKCC2 or NCC.

1.4. Regulation of the renal cation-coupled chloride cotransporters

NKCC2 and NCC belong to the solute carrier family (SLC) 12 of the electroneutral CCC and share significant structural homology (7). Because of their important roles for the body electrolyte- and water homeostasis, both transporters are subjected to an effective endocrine regulation on the transcriptional, translational and posttranslational levels (32). Transcriptional regulation, leading to changes in NKCC2 and NCC abundance, often occurs as a chronic adaptation to various alterations in the body salt balance. More rapid regulatory processes include changes of their surface abundance and phosphorylation at defined, conserved amino (N) -terminal threonine (T) - and serine (S) residues (32, 35, 36, 43). Phosphorylated, active forms of the transporters are predominantly or exclusively distributed in the apical membrane. Therefore, the surface expression and phosphorylation of NKCC2 and NCC are the final determinants of their transport activity (35, 36, 43).

1.4.1. Regulation of NKCC2 and NCC by modulation of their surface expression

The surface expression of NKCC2 and NCC depends on their processing in the endoplasmic reticulum (ER) and trans-golgi network (TGN), the rate of their exocytic movement from TGN to cell surface, as well as on the rate of their endocytic retrieval and recycling (45). This dynamic process is termed trafficking. Several hormones (e.g. AVP, Angiotensin II (Ang II), parathyroid hormone (PTH), Glucagon, ß-adrenergic agonist) have been shown to effectively modulate these processes (45).

Activity of NKCC2 is largely dependent on the intracellular cAMP level (7). Accordingly, AVP and other hormones that increase cAMP release have been established as potent activators of the transporter, mediating NKCC2 trafficking (7, 43) (Fig. 5). Increased cAMP levels stimulate luminal trafficking and membrane insertion of NKCC2. Recent studies have demonstrated that this process is, at least in part, mediated by the activation of the protein kinase A (PKA) and recruitment of two vesicle-associated membrane proteins, VAMP2 and VAMP3 (43, 45, 46). The role of PKA was confirmed by several studies using PKA inhibitors and agonists (47). Less is known about pathways mediating the internalization of the transporter (45). The few available studies suggest a dynamic nature of the cellular NKCC2 turnover with large rates of constitutive endocytosis and recycling (45, 46). It is not clear in detail which pathways are involved in NKCC2 endocytosis and whether cAMP via PKA stimulates recycling of the transporter from the subapical pool (45). Apart from cAMP, several other second messengers, like the cyclic guanosine monophosphate (cGMP), calcium, or nitric oxide (NO), have been shown to modulate NKCC2 activity in part by affecting its surface expression (48). They may either interact with the cAMP signaling or act independently (48).

Despite the fact that NCC is closely related with NKCC2 and the expression of V2R was detected in both TAL and DCT, it is not clear at present whether AVP-V2R-cAMP-PKA signaling significantly contributes to the apical trafficking of NCC as it does for NKCC2 (49). However the RAAS can effectively modulate NCC surface abundance (50).

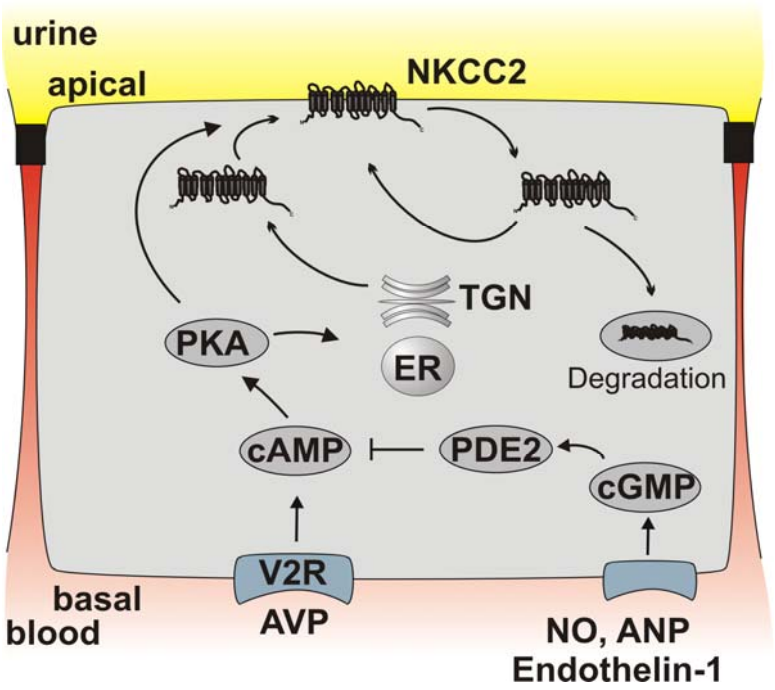

Figure 5: Simplified scheme of NKCC2 regulation in TAL.

NKCC2 is synthesized in the endoplasmic reticulum (ER) and processed in trans-Golgi network (TGN). The surface NKCC2 expression depends on the rates of its exo- vs. endocytosis and recycling to the membrane. Activation of the vasopressin type 2 receptor (V2R) facilitates apical trafficking and of NKCC2 via the cAMP/PKA pathway (45). In contrast, nitric oxide (NO), atrial natriuretic peptide (ANP), or endothelin-1 is known to increase cyclic guanosine monophosphate (cGMP) which results in stimulation of phosphodiesterase 2 (PDE2) and subsequent decrease of cAMP levels and surface expression of NKCC2. Adapted from ref. 45.

On the cellular level, trafficking and cellular abundance of NCC are controlled by *With No Lysine* [K] (WNK) kinases. WNKs are atypical protein kinases which owe their name to an unusual placement of the catalytic lysine in subdomain I instead of II. Four mammalian WNK kinases have been identified (WNK1-WNK4), each of them encoded by a separate gene (51). In recent years it has become clear that WNKs regulate renal ion transport via both catalytic and noncatalytic mechanisms (52). Regulation of some distal transport proteins, like the rat outer medullary potassium channel (ROMK) and ENaC, by WNKs requires their scaffolding rather than catalytic actions, whereas regulation of NCC occurs in a catalytic manner in that WNKs phosphorylate and activate SPAK and OSR1 which in turn bind to and phosphorylate NCC at conserved N-terminal threonine and serine residues (T53, T58, and S71, based on the mouse NCC sequence) (51, 53). The phosphorylation of the transporter may affect its surface expression since previous work suggested that interactions of NCC with adaptor protein

3 (AP3) and Sortilin (Sort) may depend on the NCC phosphorylation at T58 (54-57). Further insights were provided by identification of WNK1- and WNK4 mutations in humans responsible for the syndrome of familial hyperkalemic hypertension (FHHt), also known as Gordon's syndrome or pseudohypoaldosteronism type II (PHAII), a disease characterized by hypertension and disturbed ion homeostasis (58). Although the pathogenetic mechanisms of this disease remain to be determined in detail, it is clear that the increased sodium reabsorption through NCC plays a major role here (51, 58). This view is strongly supported by effective correction of FHHt in patients by low doses of thiazide, a blocker of NCC (59). Accordingly, mouse models of FHHt revealed an increased abundance, surface expression, and activity of NCC (60, 61).

1.4.2. Regulation of NKCC2 and NCC by phosphorylation

In recent years, several conserved N-terminal threonine- or serine residues have been identified as phosphorylation sites modulating the activities of NKCC2 and NCC (62-64). These phosphorylation sites include S87, T91, T96, T101, S126 and S874 in mouse NKCC2 and T53, T58, and S71 in mouse NCC. The individual contributions of each site to the activity of the transporters are still incompletely resolved, but phosphorylation of T96 and T101 in NKCC2 and phosphorylation of the analogous residues in NCC (T53 and T58) in response to low chloride or hypotonicity was regularly documented along with the increased activities of the transporters (62-64). Interestingly, AVP-induced activation of NKCC2 is also associated with its increased phosphorylation at T96 and T101 suggesting a functional relevance of these two residues (43). Although the effect of T96/101-NKCC2 phosphorylation on NKCC2 trafficking and activity has not so far been studied in TALs or polarized cells, experiments in frog oocyte and nonpolarized mammalian cells provide additional supporting evidence that phosphorylation of the transporter at T96 and T101 facilitates its function (62, 64, 65). The same applies to the phosphorylation of NCC at the conserved T53, T58, and S71 residues. Studies in oocytes and nonpolarized mammalian cells have linked these phosphoacceptor sites with the activity of the transporter (66). These studies suggested that the phosphorylation of T58 is particularly important for NCC activation, since mutations at this site markedly decrease NCC activity (67). Interestingly, in some patients suffering from Gitelman's syndrome, mutations in human T58 homologue, T60, have been

identified (68). Less was known about the endocrine control of NCC phosphorylation. In particular, no information was available on the respective effects of AVP.

1.4.2.1. Phosphorylation of NKCC2 and NCC by SPAK and OSR1 kinases

WNK kinases interacting with two Ste20-related kinases, SPS-related proline/alanine-rich kinase (SPAK) and oxidative stress responsive kinase 1 (OSR1), have recently been identified as key components of hormonal signaling in the distal nephron (Fig. 6).

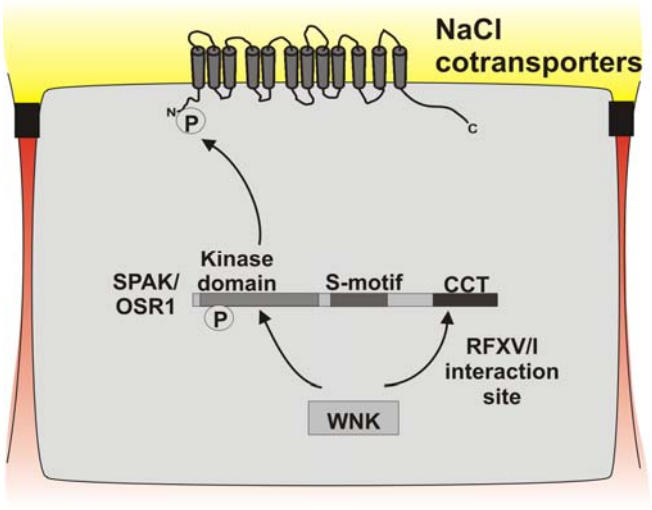

Figure 6: Schematic diagram of NKCC2 and NCC activation.

'With No Lysine K' (WNK) kinases bind SPS-related proline/alanine-rich kinase (SPAK) and oxidative stress response kinase-1 (OSR1) by RFXV/I motif in the C-terminal CCT domain and activate them by phosphorylation of threonine T233 and T185 in the kinase domain, respectively. Upon activation, SPAK and OSR1 phosphorylates the N-terminal serine and threonine residues, and thus activates, NaCl-cotransporters. Adapted from ref.18.

SPAK and OSR1 are capable of direct interactions with NKCC2 and NCC and phosphorylation of these transporters at the conserved N-terminal threonines and serines highlighted above (T96, T101, and T111 of NKCC2 and T53, T58, and S71 of NCC (51, 66). The two kinases belong to the GCK (germinal center kinase) subfamily of the STE20 family of MAPK (mitogen-activated protein kinase)-like protein kinases and share 66% identity (69-71). They are widely expressed in many tissues, including kidneys (69-71). In the kidney, expression of OSR1 was detected all along the nephron, whereas expression of SPAK was limited to TAL and DCT (72-74). An interaction of the conserved C-terminal docking site of SPAK and OSR1 with the RFXV/I binding motif

present in the downstream NKCC2 and NCC, as well as in the upstream WNKs enables the two kinases to mediate effects of WNKs on the transporters, thus making them a central piece in the WNK-SPAK/OSR1-NKCC2/NCC signaling (66, 67, 71). WNK kinases phosphorylate SPAK and OSR1 within their catalytic (T-loop) and regulatory domains (S-motif) (69). Mutations of the phosphoacceptors T243 within the catalytic domain of SPAK or T185 within the catalytic domain of OSR1 to alanines (to mimic constitutive dephosphorylation) prevented WNK-dependent activation of the kinases and, consequently, the downstream phosphorylation and activation of CCC by the mutated SPAK or OSR1 (53, 69). Accordingly, generation and characterization of $SPAK^{A243/A243}$-knockin mice, in which the wild-type SPAK was replaced by a mutant kinase mimicking constitutive dephosphorylation at T243, revealed impaired phosphorylation of NKCC2 and NCC, thus confirming the critical role of this phosphoacceptor for the catalytic activity of SPAK (56, 67). Homozygous inactivation of OSR1 in mice resulted in their prenatal lethality probably due to negative effects of this manipulation on the central nervous system (57). Less is known about the role of the regulatory domains of SPAK and OSR1. In SPAK, S383 of the regulatory domain is located in a putative autoinhibitory domain, and site-directed mutagenesis studies revealed that phosphorylation of this residue facilitates kinase activity probably due to abolishing autoinhibition (71). In contrast to SPAK, substitution of the analogous residue S325 in OSR1 to alanine to mimic its constitutive dephosphorylation did not affect the OSR1 kinase activity (57). Overall, these data led to a linear model of WNK → SPAK/OSR1 → NKCC2/NCC signaling in which WNKs phosphorylate and activate SPAK-OSR1, which in turn phosphorylate and activate NCC and NKCC2 (51,52). This view was, however, challenged by the unexpected renal phenotype of SPAK-deficient mice generated by two independent groups (56, 67). In contrast to $SPAK^{A243/A243}$-knockin mice, only the phosphorylation of NCC was markedly reduced in SPAK knockout kidneys, whereas phosphorylation of NKCC2 was strongly increased (56, 67). Although both mouse models presented with a Gitelman-like syndrome, salt loss was less pronounced in SPAK-/- compared to $SPAK^{A243/A243}$-knockin mice (56, 67). Thus, deletion of SPAK and inactivation of SPAK have similar effects on NCC, but divergent effects on NKCC2 (56, 67, 75). Like homozygous OSR1-inactivation, OSR1-deletion resulted in embryonic death (57). However, recent successful generation of viable kidney-specific (KS) OSR1-/- mice clearly demonstrated that the prenatal lethality of the

total OSR1-knockout mice was not related with the renal effects of OSR1deficiency (57). Evaluation of KS-OSR1-/- mice suggested a prominent role of the kinase in the regulation of NKCC2 but its minor effects on NCC (57). Therefore, despite significant homology between SPAK and OSR1 and their overlapping renal distribution, the available data points to distinct and non-redundant roles of the two kinases in the distal nephron (75). The mechanisms responsible for the divergent effects of SPAK and OSR1 on the distal transporters have been partially addressed and are discussed in the present work. In contrast to known genetic syndromes caused by mutations of WNKs, NKCC2 or NCC, no disease-causing mutations of SPAK or OSR1 were identified so far. However, recent Genome Wide Association Study in the Amish has identified association between single nucleotide polymorphism (SNP) in the STE39 gene (encoding SPAK) and hypertension (76). Overall, the physiologic importance of the two kinases for regulation of the distal salt transporters is beyond any doubt, while information on their regulation is rather scarce. Intracellular trafficking of SPAK and the role of a VPS10P domain receptor SORLA herein were addressed in one study (77). Another study provided evidence for positive effects of a glycosylphosphatidylinositol (GPI)-anchored Tamm-Horsfall protein (THP) abundant in TAL on the phosphorylation of NKCC2 implicating its potential interference with the relevant kinases (78). Little information was available on the systemic regulation of WNK-SPAK/OSR1 signaling, in particular by AVP.

1.4.2.2. SPAK/OSR1-independent phosphorylation of NKCC2/NCC

Existence of SPAK/OSR1-independent pathways phosphorylating NKCC2 has become evident after the identification of SPAK/OSR1-independent phosphoacceptor sites in the N- and C-termini of the transporter (S126 and S874 based on mouse NKCC2 sequence; 65). Phosphorylation of both serines is facilitated by the V2R-agonist dDAVP, as previously demonstrated *in vivo* and *in vitro* (79). Although the kinases involved in the phosphorylation of these serines have not been definitively characterized, several lines of evidence suggest a role of the AMP-activated kinase (AMPK) herein (65) (Fig. 7). Other relevant kinases, like PKA, may also be involved in the phosphorylation of SPAK/OSR1-independent phosphoacceptors plus the established targets of SPAK/OSR1 (64). Less information exists concerning the SPAK/OSR1-independent regulation of NCC. However, considering the drastic decrease of NCC abundance and

phosphorylation in SPAK$^{A243/A243}$-knockin and SPAK-/- mice, the physiologic relevance of potential SPAK-independent pathways is questionable (64, 66, 75).

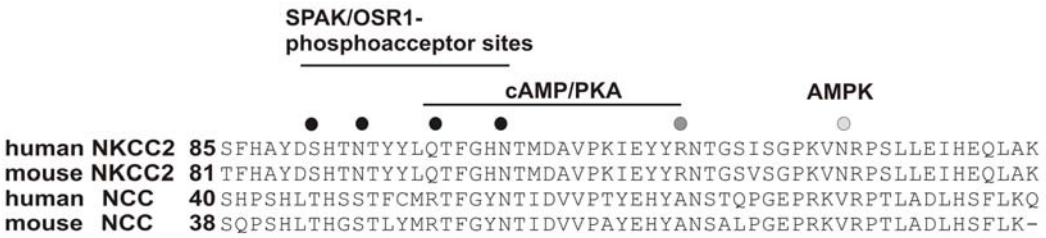

Figure 7: NKCC2 and NCC activation.

Sequence alignment of the N-terminal region of NKCC2 and NCC that are regulated by phosphorylation. Adapted from ref. 45, 64, 66.

1.5. Aims of the study

The members of the CCC family, NKCC2 and NCC, are crucial players in the regulation of renal salt excretion and maintaining arterial pressure. Their activity is subjected to strict endocrine control by AVP and RAAS which often act synergistically. These hormones effectively modulate surface expression and phosphorylation of the two transporters, thus adapting the levels of their active form in the apical membrane. So far, little information was available about the cellular pathways mediating the endocrine effects to the transporters. Recent research has unraveled the ability of two homologous Ste20-like kinases, SPAK and OSR1, to directly bind to CCC and to modulate their activity by phosphorylation of their conserved N-terminal threonine or serine residues. The specific role of these kinases in the distal nephron has so far been poorly characterized as well. Our study was therefore designed to elucidate the segment-specific aspects of the regulation of NKCC2 and NCC by AVP. Our first goal was to clarify whether the surface expression and/or phosphorylation of NCC is regulated by AVP, as has been described for the closely related NKCC2. Next, we aimed at characterizing the roles of SPAK and OSR1 in the regulation of NKCC2 and NCC at baseline and upon AVP using SPAK-deficient mice and AVP-deficient rats receiving the AVP analogue dDAVP in acute and chronic modes. This study was therefore meant to provide new information on segment-specific effects of AVP regarding NaCl reabsorption along the distal nephron *in vivo*.

2. Materials and methods

2.1. Animals, tissues, treatments

To study AVP effects on NCC adult (10–12 wk), male DI rats (Harlane; n = 25) and Wistar rats (Charles River, Sulzfeld) (n = 4) were obtained from the local animal facility (Charité Berlin) and kept on standard diet and tap water (80). DI rats received a supraphysiological and a physiological dose of dDAVP (1 ng/g or 0.3 pg/g body weight) or saline (vehicle) by intraperitoneal injection.

To prepare suspensions of renal tubules, pieces of cortex from Wistar rats were digested with a mix of type II collagenase (306 U/ml; Pan Biotech) and type XIV protease (9.4 U/ml; Sigma) for 15 min at 37°C. The resulting tubular suspensions were washed and then incubated with dDAVP (10^6 M) in renal epithelial growth medium (REGM; Lonza) or REGM alone. Suspensions were kept at 37°C for 30 min under agitation and then fixed in 3% paraformaldehyde (PFA) and placed on microscopic slides coated with poly-L-lysine for immunohistochemical analysis.

Generation of SPAK knockout (SPAK-/-) mice was described previously (71). Briefly, the SPAK gene was disrupted by duplicating exon 6 and inserting tyrosinase, neomycin resistance, and 50 HPRT genes between the two exons. Animals carrying the mutant allele were identified by PCR genotyping of tail DNA, and final determination of genotype was performed by western blotting of kidney protein lysates following sacrifice. To evaluate the role of SPAK and OSR1 in AVP signaling, SPAK knockout mice and DI rats were divided into groups (n=8 for mice [4 mice for morphological- and 4 mice for biochemical evaluation] and n=5 for rats [biochemical analysis only]) receiving dDAVP (1µg/kg body weight) or vehicle (saline) for 30 min by intraperitoneal injection. A supraphysiologic dose was chosen in order to reach saturation of AVP-signalling, since SPAK-/- had lower baseline AVP levels than WT mice (0.7 vs. 1.5 ng/ml; $p<0.05$). Plasma AVP levels were determined using ELISA (Phoenix Pharmaceuticals, Burlingame); to this end, blood was collected from the vena cava concomitantly with organ removal. For the long term study of AVP, WT- and SPAK-/- mice and DI rats were divided into groups receiving 5 ng/h dDAVP or saline as vehicle (n=3 in each group of mice and n=6 in each group of rats) for 3 days via osmotic minipumps (Alzet). Rats received normal food and tap water ad libitum. Mice received a

water-enriched food in order to keep endogenous AVP levels low. Mice received this food (21g/animal) for 3 days before implantation of the minipumps and during treatment. After minipump implantation, mice were individually placed in metabolic cages and urines were collected during the last 24 hours of the experiment. Plasma and urine sodium, potassium, chloride, and creatinine concentrations were determined and the fractional excretion (FE) of electrolytes calculated.

For morphological evaluation, animals were anesthetized by an intraperitoneal injection of pentobarbital sodium (Nembutal, 0.06 mg/g body wt, Sanofi-CEVA, Bed Segeberg). The kidneys were perfused retrogradely through the abdominal infrarenal aorta using PBS (phosphate buffered saline)/ sucrose adjusted to 330 mosm/kg H2O, pH 7.4, for 15 s, followed by 3% PFA in PBS for 5 min. Under pressure of 2 meter of water for mice and 2.20 meter for rats, animals were perfused, after opening the V. cava inferior. Kidneys were removed, dissected, and shock-frozen in liquid nitrogen-cooled isopentane (13, 15). For biochemical analysis, mice and rats were sacrificed and the kidneys removed. All experiments were approved by the Berlin Senate (permission GO 062/05 and GO 0285/10) and OHSU Institutional Animal Care and Usage Committee (Protocol A858).

2.2. Immunohistochemistry

Rabbit antisera directed against N-terminal phosphorylation sites of rat NCC (anti-phospho-T53 [pT53-NCC], anti-phospho-T58 [pT58-NCC] and anti-phospho-S71 [pS71-NCC]; all 1:1500 dilution, gift from S. Uchida, Tokyo, Japan; 56, 57, 80), guinea pig anti-NKCC2 antibody directed against N-terminal 85 amino acids (1:1000 dilution; gift from D. H. Ellison, Portland, Oregon; 36), pNKCC2 (anti-pT96/pT101-NKCC2, 1:2000 dilution, gift from D. H. Ellison, Portland; 41), rabbit anti-NCC antibody (1:1000 dilution; gift from D. H. Ellison; 80), SPAK (C-terminal antibody from Cell Signaling and N-terminal antibody from Santa Cruz Biotechnology; 69), OSR1 (D.R. Alessi, Dundee, UK; 69) and phosphorylated SPAK/OSR1 (pT243-SPAK/pT185-OSR1; antibody recognizes pT243 of mouse SPAK and pT185 of mouse OSR1 [T-loop] and pS383-SPAK/pS325-OSR1; antibody recognizes pS383 of mouse SPAK and pS325 of mouse OSR1 [S-motif], both gift from D.R. Alessi, Dundee, UK; 69) were the primary antibodies used. All antibodies have been published. For detection of phosphorylated kinases and

transporters, antibodies were preabsorbed with corresponding, non-phosphorylated peptides in 10-fold excess before application. Sets of cryostat sections from each experiment were processed exactly in the same fashion with samples from the compared groups placed on the same slide. 5mm sections, washed three times with 1xPBS, incubated in 1xPBS with 0.5% Triton for 30min, washed in PBS, blocked in 5% milk in PBS (30 min), and incubated with primary antibody diluted in 5% milk in 1xPBS (1 h). For multiple staining, antibodies were sequentially applied, separated by a washing step. Fluorescent Cy2-, Cy3 or Cy5-conjugated antibodies (DIANOVA) or HRP-conjugated antibodies (Santa Cruz Biotechnology) were used for detection. Sections were washed and coverslips applied with PBS-glycerol.

Intensity of confocal fluorescent signals was scored across each profile using a Leica DMRB microscope equipped with a SPOT 32 camera and MetaView 3.6a software (Diagnostic Instruments, Universal Imaging) or a Zeiss confocal microscope (LSM 5 Exciter) and ZEN 2008 software (Zeiss). At least 20 similar tubular profiles were evaluated per individual animal. Intensities of the confocal fluorescent signals were scored across each profile using ZEN2008 software (Zeiss), and mean values within 2 µm distance at the apical side of each tubule were obtained. Background fluorescence levels were determined over cell nuclei and subtracted from the signal.

2.3. Ultrastructural analysis

For immunogold evaluation of NKCC2 and NCC, perfusion-fixed kidneys were embedded in LR White resin. Ultrathin sections were incubated with the respective primary antibody. Signal was detected with 10 nm nanogold-coupled secondary antibody (Amersham) and visualized using transmission electron microscopy. Quantification of immunogold signals in TAL and DCT profiles was performed on micrographs recorded at x16,700 and printed at x50,000 magnification according to an established protocol (50). From each animal at least 10 profiles and 4 to 5 cells per profile were analyzed from sections oriented approximately at right angles to the apical cell membrane and showing negligible background over mitochondria and nuclei. Evaluation was performed in a blinded fashion. Gold particles were attributed to the apical cell membrane when located near (within 20 nm of distance) or within the bilayer;

particles found below 20 nm of distance to the membrane up to a depth of 2 µm or until the nuclear envelope were assigned to cytoplasmic localization.

2.4. Immunoblotting and co-immunoprecipitation

Kidney cortices were excised and homogenized in buffer containing 250 mM sucrose, 10 mM triethanolamine, protease inhibitors (Complete; Roche Diagnostics), and phosphatase inhibitors (Phosphatase Inhibitor Cocktail 1; Sigma) (pH 7.5). The homogenates were subjected to sequential centrifugation steps to obtain postnuclear fractions by removing nuclei (1,000 g, 15 min at 4°C). For the study of AVP-induced effects on NCC, additionally, vesicle-enriched fractions (removal of the large plasma membrane fragments at 17,000 g for 1 h and subsequent spinning at 200,000 g for 1 h) were separated.

The concentrations of the samples were determined by a bicinchoninic acid protein assay reagent kit (Micro BCATM Protein Assay Reagent Kit, Pierce Biotechnology, Rockford, USA). This water-soluble complex exhibits a strong absorbance at 562 nm that is linear with increasing protein concentrations. The samples were incubated at 37°C for 2 hours, following a cool-down to room temperature. To determine the protein concentration of each unknown sample, a standard curve was used by plotting the average blank-corrected 562 nm reading for each BSA standard vs. its concentration in µg/ml.

The samples were dissolved in a buffer (2 % SDS, 10 % glycerol, 5 % ß-mercaptoethanol, 1 % bromphenol blue, 95 mM Tris, pH 6,8) and incubated for 15 min. at 65°C. The samples were separated by PAGE (buffer: SDS 0,1 %, glycin 192 mM, Tris 25 mM; pH 8,3; 8–10% acrylamide gel; 50 µg protein/lane). The molecular weight was determined with a marker (Dual Precision Marker, Bio-Rad Laboratories, Hercules CA, USA).

After electrophoretic transfer to a polyvinylidene fluoride membrane (Schleicher und Schüll, Dassel) with western blotting in a Tank-Sandwich-System (Bio-Rad-Laboratories), equity in protein loading and blotting was verified by membrane staining using 0.1% Ponceau red staining. After they were blocked in 5% milk for 1 hour, polyvinylidene fluoride membranes were incubated with primary antibodies against

NKCC2, pT96/T101-NKCC2, NCC, pT58-NCC, pT71-NCC, SPAK, pSPAK-OSR, β-actin (Sigma), or GAPDH (Santa Cruz Biotechnology), each for 1 h at room temperature, then incubated overnight at 4°C and then, after several washing steps, exposed to HRP-conjugated secondary antibodies (1:3000; Dako Cytomation) for 2 h at room temperature. Immunoreactive bands were detected by chemiluminescence (ECL, Amersham, Freiburg), exposed to X-ray films (Hyperfilm ECL), and the signals scanned and densitometrically evaluated. Monoclonal mouse anti-actin antibody (Sigma) was used to normalize all data for expression of the housekeeping gene actin. The linear range of the detection was controlled by reducing the load of the postnuclear homogenates to 50%, which produced corresponding decreases of target protein (80).

Immunoprecipitation (IP) of NKCC2 from rat medullary kidney homogenates or NCC from rat cortical homogenates was performed overnight at 4°C in TBS/tween (0.5% tween-20) buffer using anti-NKCC2 (Millipore) or anti-NCC antibodies (19) covalently bound to Dynabeads® M-270 Epoxy (Invitrogen). The co-immunoprecipitated products were detected by immunoblotting as described above.

2.5. Morphometric procedures

The fractional volume of DCT segments among strains was measured with a light microscope according to previously characterized methods (81). Briefly, 5 mm-thick paraffin sections were stained for NCC to identify DCT. Cortical areas extending between the renal capsule and the outer medullary boundary were evaluated. Sections were photographed and printed at a final magnification of 3100. At least five prints per animal were evaluated.

2.6. Cloning of rat KS-SPAK

For identification of alternatively spliced KS-SPAK in rat kidney cDNA primers were designed based on alignment of rat intron 5 with mouse exon 5A sequence and two primer pairs were selected from regions of aligned sequence with low homology to mouse exon 5A to reduce the possibility of amplifying mouse cDNA (forward primer 5´ CATGTGTATGCCAGATTCATCTCGAAAGAG 3´ [putative exon 5A] + reverse primer 5´ GGGCTATGTCTGGTGTTCGTGTCAGCA 3´ [exon 10], predicted PCR product size 510 bp and forward primer 5´ CCCAGGCTTTGTGGCTTTGGGTAAC 3´ [putative exon

5A] + reverse primer 5´ CAGGGGCCATCCAACATGGGG 3´ [exon 6], predicted PCR product size 363 bp). RT-PCR was performed using total RNA extracted from whole rat kidney. PCR products were cloned into pGEMT-easy vector and verified by sequencing.

2.7. Analysis of data

Results were evaluated using routine parametric statistics. Groups were compared by means of the Student *t* test or, if the data violated a normal distribution, the nonparametric Mann–Whitney test. Two-way ANOVA with Bonferroni correction was employed to analyze differences in the effect of dDAVP between WT and SPAK-/- genotypes. A probability level of $p<0.05$ was accepted as significant. All results are expressed as the means ± SD.

3. Results

3.1. AVP activates NCC by stimulating its luminal trafficking and phosphorylation

Short-term administration of the V2R agonist dDAVP promotes significant trafficking of NKCC2 to the luminal membrane in mouse (43) and rat kidney (36, 41). To evaluate AVP induced effects on DCT, NCC was analyzed in DI rats receiving dDAVP or vehicle for 30 min. DI rats responded significantly to externally administrated AVP, making them an ideal animal model to study dDAVP effects.

Confocal and electron microscopic evaluation of intracellular NCC distribution in DCT profiles from vehicle- or dDAVP-treated DI rats revealed significant increases of NCC signal in the apical membrane in the treated groups (Fig. 8A-D). Quantification of the NCC immunogold labeling showed that the intracellular distribution of gold particles had shifted significantly to the apical plasma membrane of the dDAVP- vs. vehicle-treated groups (79 ± 12% vs. 56 ± 17% of total NCC immunoreactivity, respectively, $p<0.05$ (Fig. 8E).

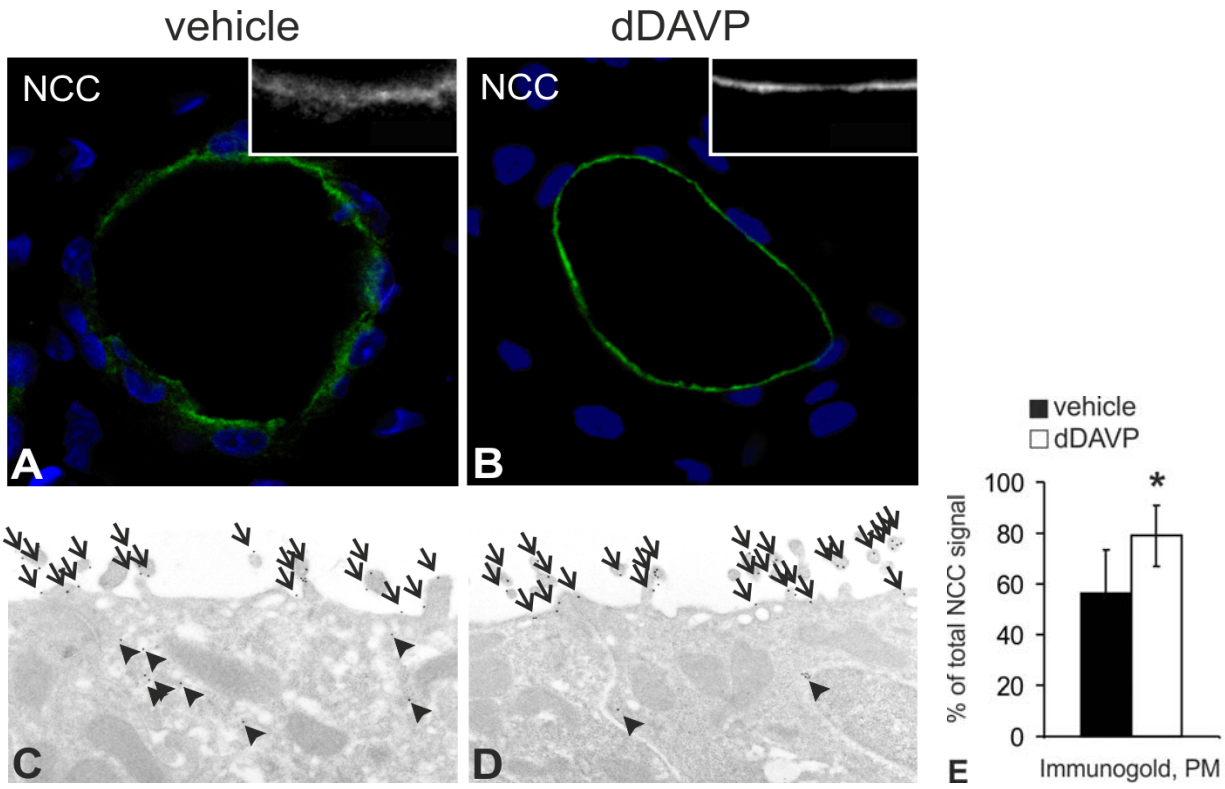

Figure 8: Effects of dDAVP on NCC trafficking.

(A, B) Representative confocal images of DCT from DI rats showing signal for NCC (green) and counterstained nuclei (blue). Inserts demonstrate apical cellular aspect at higher resolution. (C, D) NCC signal (5 nm gold particles) at apical membrane (arrows) and subapical vesicles (arrowheads) of DCT. (E) Numerical evaluation of NCC immunogold signal at the plasma membrane (PM). Data are means ± SD from n =5 rats/group; *p< 0.05; original magnification x630 (A, B) and x16,700 (C, D). From ref. 80.

Densitometric quantification of NCC signal intensity in vesicle-enriched fractions from kidney cortex supported the results of the immunocytochemical analysis; dDAVP leads to a significant decrease of NCC signal in the vesicle-enriched fractions (-33± 9%; p< 0.05) without concomitant change of total NCC abundance (Fig. 9 A, B).

Next, acute effects of dDAVP on NCC phosphorylation were evaluated. Immunoblotting of kidney extracts from vehicle- and dDAVP-treated DI rats using antibodies to pT53-NCC and pS71-NCC revealed significant increases of NCC phosphorylation upon dDAVP (+147% for pT53-NCC and +42% for pS71-NCC respectively; p< 0.05, Fig. 10 A, C, D).

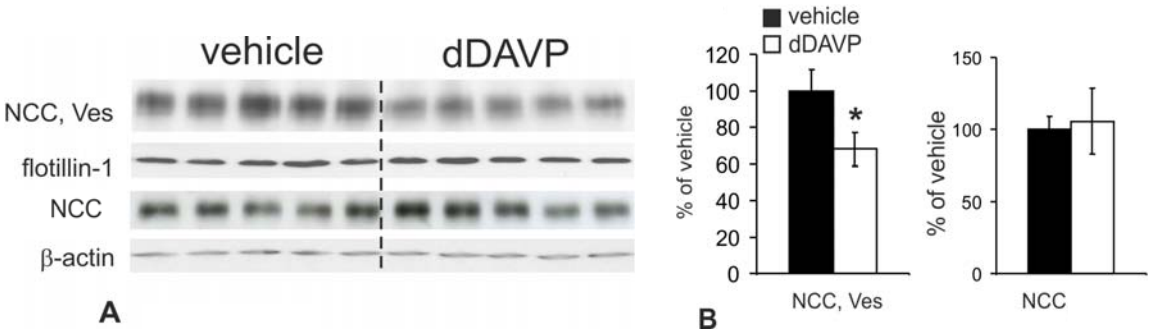

Figure 9: Effects of dDAVP on NCC distribution.

(A) Western blots showing NCC immunoreactivity (approximately 160 kDa) in vesicle-enriched (Ves) and whole kidney cortical homogenates with corresponding loading controls flotillin-1, (~ 48 kDa) and β-actin (~ 42 kDa), respectively. (B) Densitometry of Western blot signals. Data are means ± SD from n =5 rats/group; *p< 0.05. From ref. 80.

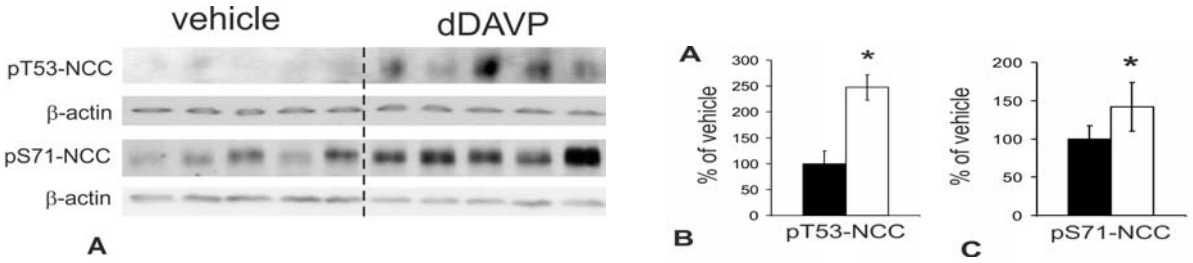

Figure 10: Effects of dDAVP on NCC abundance and phosphorylation in DI rats.

(A) Western blots from kidney cortical homogenates showing immunoreative bands for pT53-NCC and pS71- NCC (~ 160 kDa), and β-actin as loading controls (~ 42 kDa). (B, C) Densitometric evaluations of immunoreactive signals normalized for β-actin. Data are means ± SD from n = 5 rats/group; *p< 0.05 for differences between vehicle- and dDAVP-treated group. From ref. 80.

These results were supported by immunohistochemical evaluation of pNCC signals using the same antibodies. Both, pT53-and pS71-NCC signals were markedly increased in dDAVP-treated kidneys as compared to vehicle-treated kidneys (Fig. 11 A-F). Due to the fact that several phosphorylation sites, including pT53 of NCC, display significant homology between NKCC2 and NCC, cross-reactivity of the anti-pT53-NCC antibody with NKCC2 was excluded by double-staining (Fig. 11 C, D).

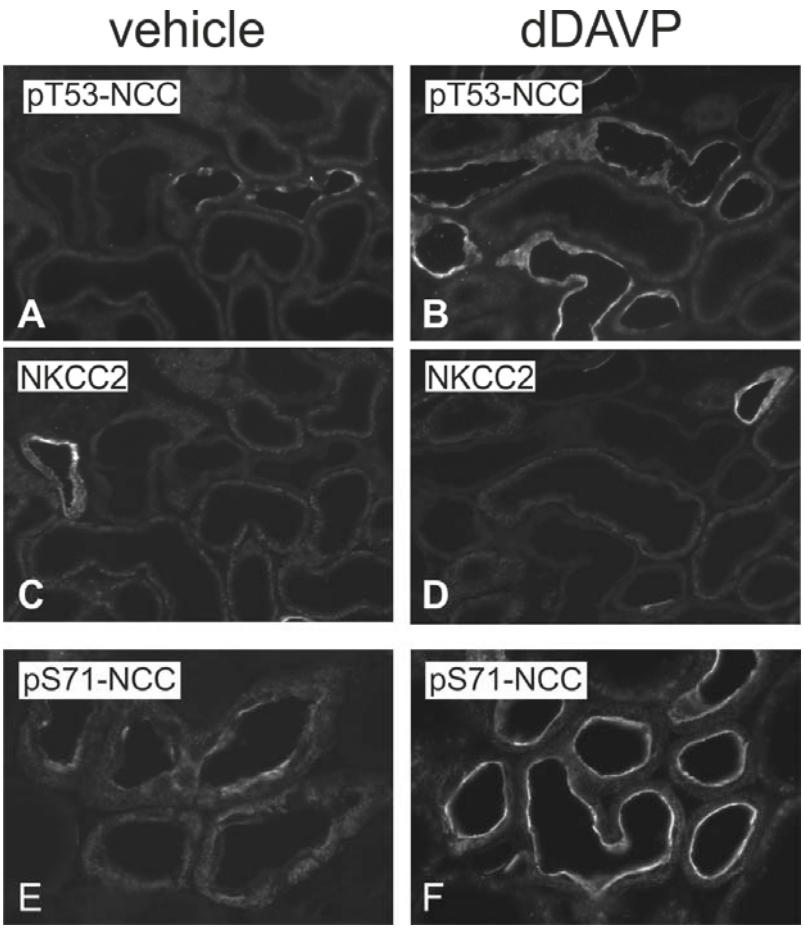

Figure 11: Immunohistochemical evaluation of dDAVP effects on NCC distribution and phosphorylation in DI rats.

(A-F) Comparative image pairs of pT53-NCC (doublestaining with NKCC2) and pS71-NCC. Original magnification x400. From ref. 80.

Systemic interactions between AVP and RAAS have been described. In DI rats, the injection of dDAVP stimulates secretion of aldosterone and Ang II. Both are strong activators of NCC (50, 84). To verify whether the observed, dDAVP-induced changes in NCC phosphorylation directly resulted from activation of V2R in DCT, we stimulated extracted renal tubules in suspension with dDAVP, thus excluding an effect of other hormones of the homeostatic control systems such as aldosterone or Ang II. Confocal evaluation of immunofluorescence intensity revealed significant increases of pS71-NCC signal in dDAVP- compared with vehicle-treated DCTs (+72 ± 22%; $p < 0.05$) (Fig. 12 A-C).

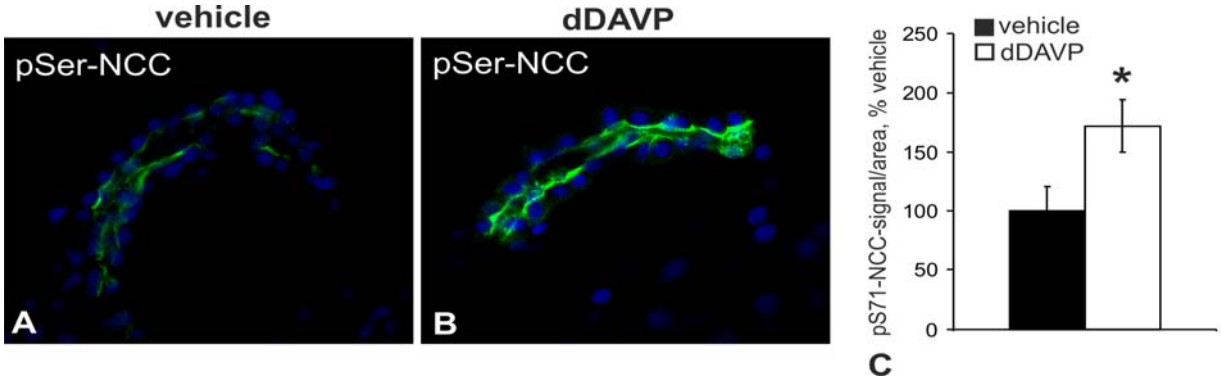

Figure 12: Effects of dDAVP on NCC phosphorylation in suspensions of cortical renal tubules.

(A, B) Confocal images of DCT profiles from tubular suspensions from Wistar rat kidneys after administration of vehicle or dDAVP (10^{-6} M; 30 min) and staining with pSer71-NCC antibody. (C) Fluorimetric evaluation of apical pS71-NCC signal intensity. Data are means ± SD from n=4 rats/group; *p< 0.05 for differences between vehicle- and dDAVP-treated groups; original magnification X400. From ref. 80.

Together, these results demonstrate that stimulation of V2R by short-term dDAVP application in DI rats induces luminal translocation and phosphorylation of known stimulatory NCC-residues, in a manner similar to that previously described for NKCC2 in an aldosterone/ Ang II- independent manner.

3.2. Homologous SPAK and OSR1 kinases distinctly regulate NKCC2 and NCC

Posttranslational regulation of NKCC2 and NCC by phosphorylation is crucial for their transport activities (62, 63). Interaction of WNK kinases with SPAK and OSR1 serves to phosphorylate NKCC2 and NCC (64, 66, 66, 71). To gain more information about the individual roles of SPAK and OSR1 kinases for the activation of NKCC2 and NCC, we studied these kinases in SPAK knockout mice (SPAK -/-) (71).

First, distribution of SPAK and OSR1 in wild-type (WT) and SPAK-/- mice was evaluated. By immunohistochemial labeling of NKCC2 and NCC, TAL and DCT was identified, respectively. In WT, antibody against the C-terminal domain of SPAK (C-SPAK) revealed strong apical signal in the TAL, whereas in the DCT, a particulate cytoplasmic signal was dominant along with weaker subapical staining in WT (Fig. 13 A, B, E, F). No signal was detectable in SPAK-/- kidneys (Fig. 13 C, D, G, H). Anti-OSR1 antibody revealed strong apical signal in TAL but weaker signal in DCT of WT (Fig. 13 I, J). In contrast to WT, the inverse OSR1 distribution pattern with diminished TAL but increased cytoplasmic and apical DCT signals was evident in SPAK -/- mice (Fig. 13 K,

L). These patterns, suggesting compensatory redistribution of OSR1 in SPAK deficiency, are schematized in Fig. 13 M.

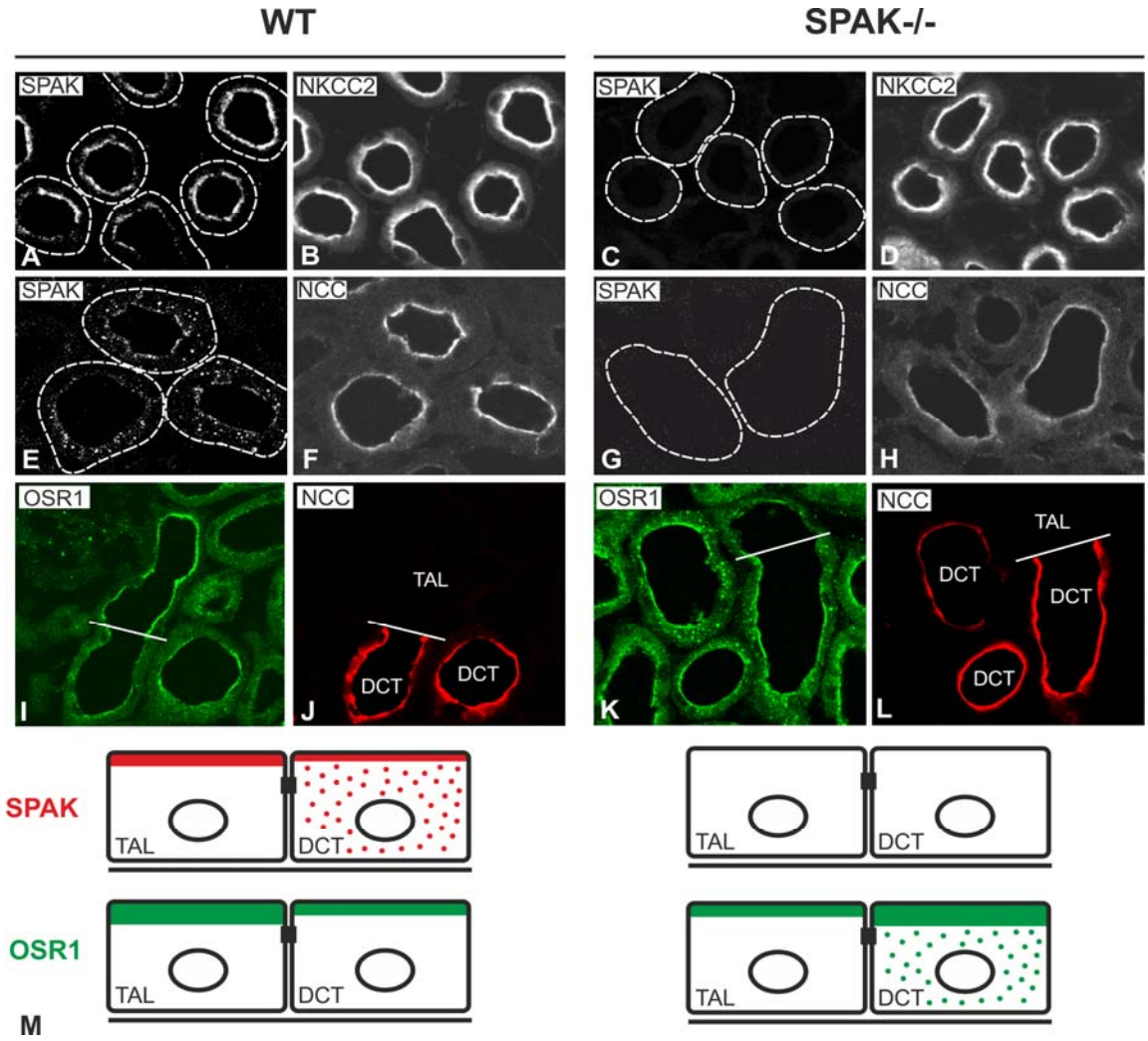

Figure 13: Distribution of SPAK in wild-type (WT) and SPAK-/- mouse kidneys.

(A-L) SPAK and OSR1 immunostaining in TAL and DCT and double-staining with segment-specific antibodies to NKCC2 for TAL or NCC for DCT. (A-H) In WT kidneys, SPAK signal in TAL is concentrated apically (A, B). DCT shows also cytoplasmic SPAK signal (E, F). Note the complete absence of SPAK signal in TAL and DCT in SPAK-deficient (SPAK-/-) kidney (C, D, G, H). (I-L) OSR1 signal is concentrated apically in TAL and DCT of WT kidneys, whereas in SPAK-/- kidneys, DCT shows additional cytoplasmic signal. Note that OSR1 signal is stronger in TAL than in DCT in WT, whereas SPAK -/- shows the inverse. Bars show TAL/DCT transitions; original magnification x400. (M) The distribution patterns of SPAK and OSR1 are schematized. From ref. 82.

To evaluate if our SPAK -/- mice model exhibit the same abnormalities in NKCC2 or NCC phosphorylation, as reported by Yang and colleagues (56), we performed western blot analysis of kidney protein homogenates from WT and SPAK -/- mice. Indeed, SPAK deficiency caused opposing baseline phosphorylation patterns of the cotransporters.

SPAK deletion led to increased phosphorylation of T96/pT101-NKCC2 signal, whereas pT58/pS71-NCC signal was substantially decreased as compared to WT mice (Fig. 14 A, B).

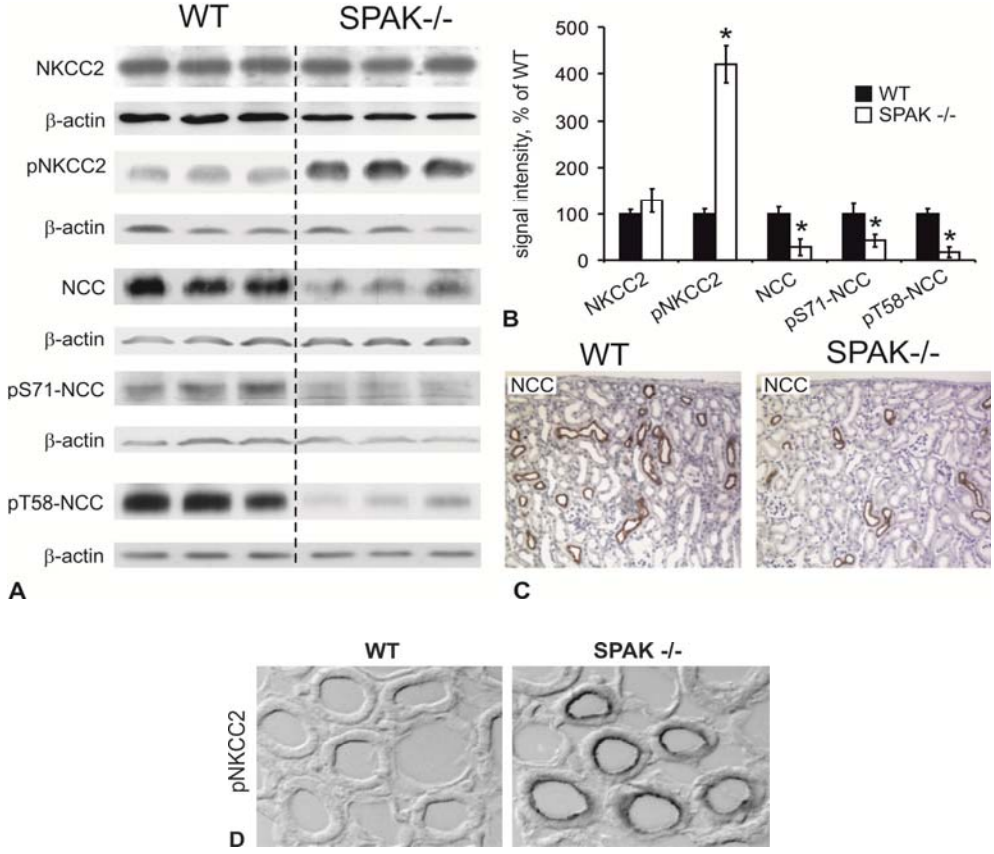

Figure 14: Steady state abundance and phosphorylation of NKCC2 and NCC in WT and SPAK-/- mice.

(A) Representative immunoblots from WT and SPAK-/- kidney homogenates detected with antibodies to NKCC2, pT96/T101-NKCC2, NCC, pS71-NCC, and pT58-NCC (bands at approximately 160 kDa throughout). Loading was controlled by concomitant detection of β-actin (approximately 42 kDa) as shown below the corresponding immunoblots. (B) Densitometric evaluation of the blots normalized to loading controls. Data are the means ± SD, * $p<0.05$. (C) Low-power images of kidney sections stained for NCC expression (brown staining) by immunohistochemistry demonstrating hypotrophy of DCT in SPAK -/- mice. Representative image pairs after pNKCC2 immunostaining of WT and SPAK-/- mice TALs. (n = 8 per group). From ref. 81, 82.

This was paralleled by an unchanged NKCC2 expression, but decreased NCC abundance (Fig. 14 A, B). Low-power immunohistochemistry suggested that the number of DCT profiles was reduced in SPAK -/- mice (Fig. 14 C). Subsequently, quantitative analysis confirmed that the fractional DCT volume (determined as the fraction of tubule that express NCC) was approximately 50% lower in SPAK -/- mice compared to WT, suggesting that decreased NCC expression was also caused by the reduction in DCT

mass in SPAK -/- mice. NKCC2 immunohistochemical phosphorylation signal in TAL profiles was stronger in WT mice than in SPAK -/- mice, supporting Western blot data (Fig. 14 D).

3.2.1. Full-length and truncated isoforms of SPAK and OSR1 have different distribution and functions in the kidney

The linear model of WNK → SPAK/OSR1 → NKCC2/NCC signaling was proposed based on the results of heterologous overexpression studies as well as on the observed decrease of NKCC2- and NCC phosphorylation in $SPAK^{A243/A243}$-knockin mice expressing a catalytically inactive mutant instead of wild-type SPAK (67). This view was, however, challenged by the confusing renal phenotype of SPAK-deficient mice showing decreased NCC phosphorylation but, unexpectedly, increased NKCC2 phosphorylation. These data suggested distinct roles of the kinase in TAL vs. DCT. One possible reason may be the occurrence of different SPAK isoforms in the two nephron segments, as has been previously described for the renal WNK1 gene, giving rise to the catalytically active long WNK1 form expressed along the whole nephron and the kinase-dead, truncated, kidney-specific variant abundant in DCT (83). To resolve this issue we have analyzed SPAK isoform expression and distribution along the distal nephron.

Previous work has demonstrated that SPAK can be generated from two translation initiation sites, resulting in a full-length SPAK (FL-SPAK) and a smaller isoform (SPAK2). The latter starts 115 amino acids downstream of the FL initiation site and was predicted to be kinase deficient due to the partial N-terminal truncation of the catalytic domain (8). However, immunoblotting using an anti-SPAK antibody recognizing the C-terminus of the kinase (C-SPAK antibody) has revealed a total of three immunoreactive products in the kidney: still another, faster migrating form suggested the existence of a third, shorter SPAK variant. For its predominant abundance in the kidney, this product was referred to as KS-SPAK (Fig. 15 A, B). Our collaboration partners searched for SPAK splice SPAK variants and indeed identified another truncated variant with the transcriptional start site located in the alternative exon 5 (Figure 16 A-D, 81). Characteristic minor bands for FL-SPAK and SPAK2, but a major band for KS-SPAK were correspondingly obtained by immunoblotting of mouse (Fig. 15) or rat kidney extracts using C-SPAK antibody (Fig. 16 B).

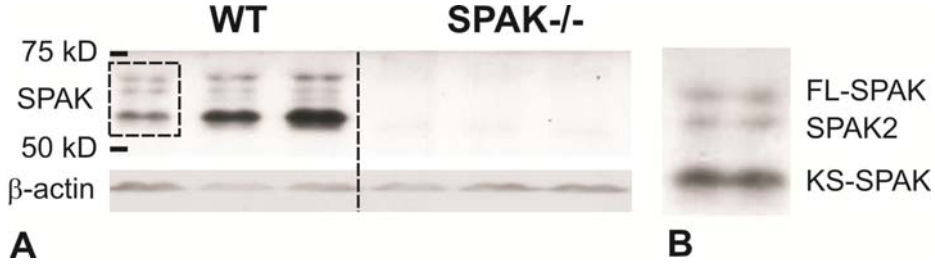

Figure 15: Detection of three SPAK isoforms in WT mice.

(A, B) SPAK runs between 50 and 75 kDa on immunoblots from WT kidney using anti-C-terminal antibody (C-SPAK). Blots typically show minor bands for full-length (FL) SPAK and a translationally truncated product (SPAK2), as well as a major band for the truncated, kidney-specific (KS) SPAK isoform. From ref. 82.

Due to the truncation, both KS-SPAK and SPAK2 are predicted to lack the N-terminus present in the full-length protein. FL-SPAK, as recognized by antibody against its N-terminal domain, was weakly expressed along TAL but well detectable along DCT. In contrast, total SPAK comprising both full-length and truncated forms, detected by an antibody against its C-terminus, was more abundant along TAL than DCT. In support of the confocal data, immunoblotting of extracts from kidney medulla (containing TAL but no DCT) using C-SPAK antibody produced major signals for KS-SPAK with only minor abundance of FL-SPAK, whereas the evaluation of renal cortical extracts (containing both TAL and DCT) revealed an inverse pattern with the predominant abundance of FL-SPAK (Fig. 17 B).

Importantly, KS-SPAK retains the C-terminal docking site responsible for interactions with the RFxV/I domain of SPAK substrates (66). Activating and inhibitory SPAK forms may therefore compete for the binding with NKCC2. Moreover, synthetic, kinase-dead SPAK mutants have shown dominant-negative effects on the activity of FL-SPAK (74). In line with this, our collaboration partners have described the dominant-negative effects of KS-SPAK on the phosphorylation of NKCC2 and NCC by FL-SPAK in vitro as well as in cultured cells (81).

Together, our results are in line with the hypothesis that distinct expression of the catalytically active FL-SPAK and the kinase-deficient, dominant-negative KS-SPAK are responsible for the opposite effects of SPAK-deletion in TAL vs. DCT. Whereas in SPAK -/- mice the deletion of FL-SPAK prevents the activation of NCC, the absence of inhibitory KS-SPAK facilitates the activation of NKCC2 by the homologous OSR1 kinase which is abundantly expressed in TAL (81, Fig. 18).

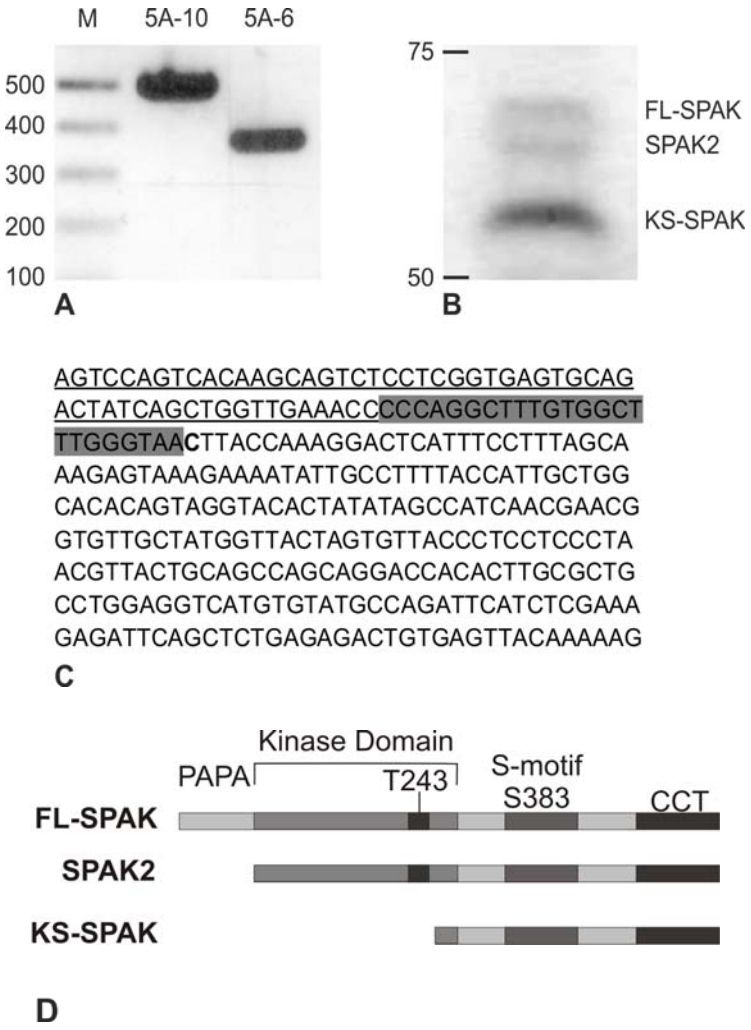

Figure 16: Verification of KS-SPAK expression and abundance in rat kidney.

(A) RT-PCR from total rat kidney RNA using forward primer in the alternative exon 5 (5A) of KS-SPAK and reverse primers in exon 10 (5A-10) or exon 6 (5A-6) produced products of predicted sizes (M = DNA ladder). (B) Immunoblotting from rat kidney homogenates using C-SPAK antibody produced the characteristic three bands corresponding to FL-SPAK, SPAK2, and KS-SPAK. Note high abundance of KS-SPAK. (C) Sequencing of both KS-SPAK PCR products (A) confirmed the expression of this splice variant in rat kidney. Clones contained rat exon 5A fused to rat exon 6. Shaded text indicates location of the forward primer within rat exon 5A; the underlined sequence is homologous to mouse exon 5A. (D) Schematic diagram of renal SPAK isoforms: FL-SPAK contains proline-alanine repeating sequence (PAPA) box and the kinase domain with T-243 phosphorylation site, S-motif and conserved C-terminal (CCT) domain. SPAK2 and KS- SPAK lack the N-terminus with the PAPA box which is present in FL-SPAK. Phosphorylation of SPAK at T243, and at S383 within its regulatory domain, is known to increase its activity (56, 69). From ref. 81, 82.

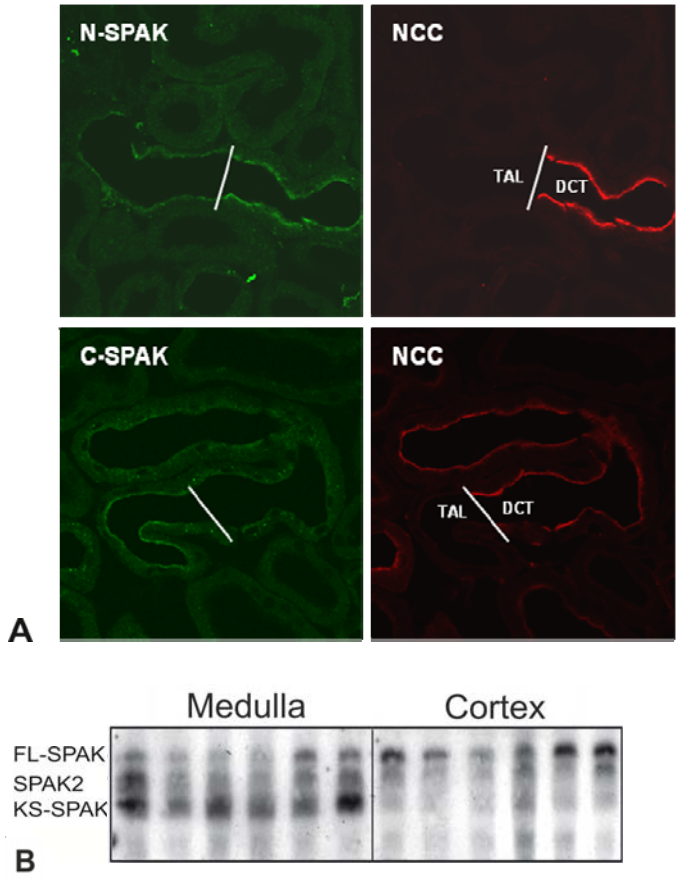

Figure 17: SPAK expression in TAL and DCT.

(A) Transitional segments (TAL/DCT) determined using anti-NCC antibody are shown. FL-SPAK (detected with anti-N-SPAK) is predominantly expressed in DCT, whereas total SPAK abundance (detected with anti-C-SPAK) is higher along TAL than DCT. (B) Total SPAK immunoblot of medulla and cortex. Note that most cortical SPAK is the FL-SPAK, whereas truncated KS-SPAK and SPAK2 are more highly expressed in medulla. From ref. 81.

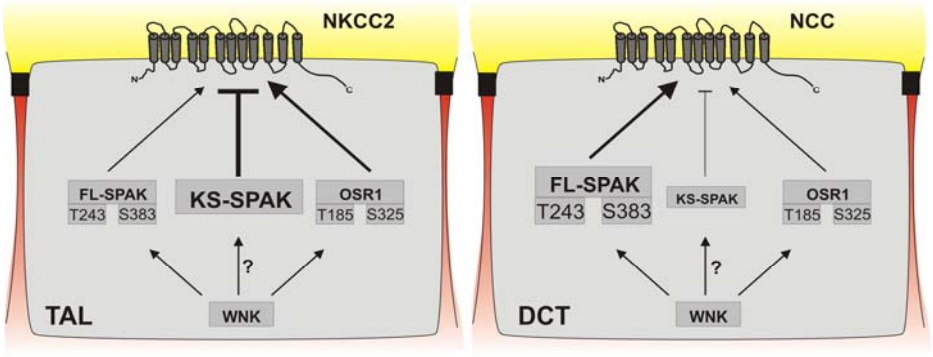

Figure 18: Proposed model of WNK-SPAK/OSR1-NKCC2/NCC signaling in the distal nephron.

Arrows indicate downstream effects, the T shape indicates inhibition. The thickness of the arrows indicates the significance of the respective kinases and their actions in phosphorylation of NKCC2 or NCC. KS-SPAK is predominantly expressed in TAL, whereas in DCT, expression of KS-SPAK is nearly absent and FL-SPAK plays the dominant role in NCC activation.

3.3. SPAK and OSR1 mediate AVP signaling

To test whether stimulation of AVP-V2R signaling induces activation of SPAK and/or OSR1, dDAVP or vehicle were administered intraperitoneally to WT and SPAK-/- mice. Before studying the AVP-effects, we examined the steady-state phosphorylation of SPAK and OSR1 within their catalytic domains (T243 in SPAK and T185 in OSR1) as an indicator of their activity (69). Staining with anti pT243-SPAK/pT185-OSR1 antibody, which recognizes the phosphorylated species of both kinases owing to the similarity of their phosphorylation sites, was absent in mTAL and weak in cTAL of both genotypes, whereas in DCT, moderate apical signal in WT, but weaker staining in SPAK-/- mice were observed (Fig. 19 A, C, E, G,, I, K, M, O, Q).

Phosphorylation of the kinases within their regulatory domains (S383 for SPAK and S325 for OSR1) may facilitate their activity as well (56), so that staining with anti pS383-SPAK/pS325-OSR1 antibody was also performed; moderate apical TAL and apical plus cytoplasmic signals in DCT were obtained in WT (Fig. 20 A, E, I, M, Q), whereas in SPAK-/-, TAL and DCT were nearly negative (Fig. 20 C, G, K, O, Q). These data agree with earlier information on low baseline phosphorylation of renal SPAK and OSR1 (73) and indicate the lack of compensatory increase of OSR1 phosphorylation in SPAK deficiency.

Next, possible effects of dDAVP were assessed. Phosphorylation of SPAK and/or OSR1 within their catalytic domains was studied with anti-pT243-SPAK/pT185-OSR1 antibody. Since immunoblotting produced unclear results in this case, confocal evaluation was preferred. mTAL and DCT demonstrated significant increases of pT243-SPAK/pT185-OSR1 signals both in WT (15-fold for mTAL and 3-fold for DCT; $p<0.05$) and in SPAK-/- mice (8-fold for mTAL and 2-fold for DCT; $p<0.05$), whereas no significant changes were detected in cTAL in either genotype (Fig. 19). Phosphorylation of the regulatory domain was detected with anti pS383-SPAK/pS325-OSR1 antibody. Here, confocal evaluation revealed an elevated signal in mTAL and DCT of WT kidneys (1.5- and 2-fold, respectively; $p<0.05$), whereas no significant changes were recorded in SPAK-/- kidneys upon dDAVP (Fig. 20). Corresponding immunoblots showed increased signals in WT but not in SPAK-/- kidneys (Fig. 21). Short term dDAVP administration thus stimulated phosphorylation of the kinases mainly in mTAL and DCT.

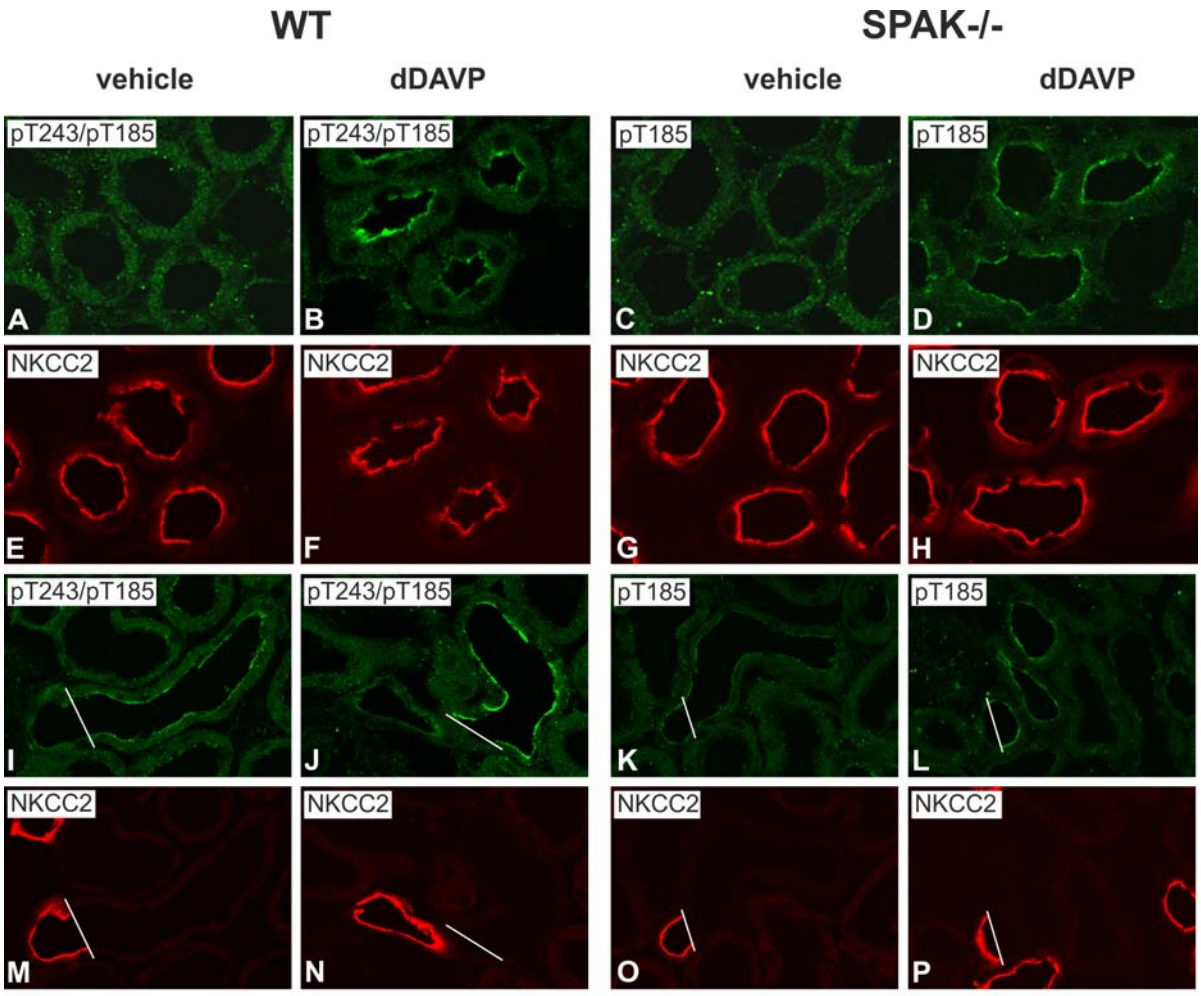

Q

	WT		SPAK-/-	
	vehicle	dDAVP	vehicle	dDAVP
mTAL	3.3 ± 1.3	44.4 ± 9.9*	3.6 ± 1.8	25.7 ± 12.5*
cTAL	14.0 ± 7.4	23.0 ± 10.7	7.4 ± 8.2	8.3 ± 4.7
DCT	31.9 ± 17.4	107.6 ± 25.1*	25.8 ± 7.1	59.7 ± 9.3*

Figure 19: Steady state and dDAVP-induced phosphorylation of SPAK and OSR1 within their catalytic domains in WT and SPAK-/- mouse kidneys, immunohistochemistry.

(A-P) Immunolabeling of pT243-SPAK/pT185-OSR1 (pT243/pT185) and double-staining for NKCC2 in renal medulla (A-H) and cortex (I-P) of vehicle- and dDAVP-treated (30 min) WT and SPAK-/- kidneys. Bars indicate TAL/DCT transitions. (Q) Evaluation of the confocal signals in mTAL and cTAL by intensity. Note more pronounced response to dDAVP in WT compared to SPAK-/- mice. Data are the means ± SD; * $p<0.05$ for intrastrain differences (vehicle vs. dDAVP). From ref. 82.

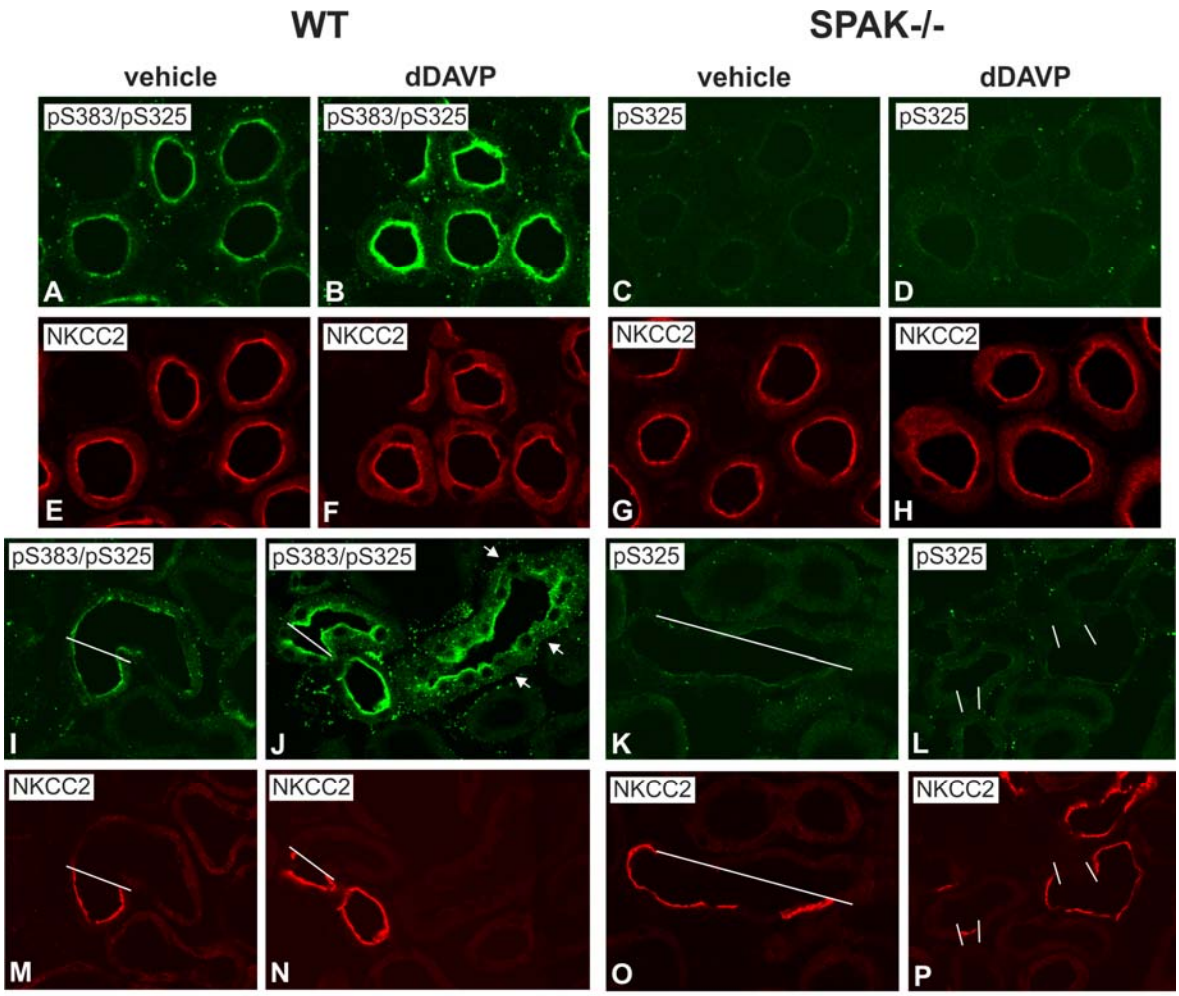

Q

	WT		SPAK-/-	
	vehicle	dDAVP	vehicle	dDAVP
mTAL	93.4 ± 13.9	149.4 ± 14.0*	6.5 ± 5.4	6.6 ± 2.3
cTAL	89.2 ± 29.3	105.9 ± 35.1	11.5 ± 3.7	9.0 ± 5.7
DCT	56.3 ± 15.2	100.0 ± 22.5*	11.0 ± 5.3	7.5 ± 1.0

Figure 20: Steady state and dDAVP-induced phosphorylation of SPAK and OSR1 within their regulatory domains in WT and SPAK-/- mouse kidneys, immunohistochemistry.

(A-P) Immunolabeling of pS383-SPAK/pS325-OSR1 (pS383/pS325) and double-staining for NKCC2 in renal medulla (A-H) and cortex (I-P) of vehicle- and dDAVP-treated (30 min) WT and SPAK-/- kidneys. Bars indicate TAL/DCT transitions. dDAVP induces increases in both early and late DCT of WT; the latter identified by the presence of intercalated cells (arrows). (Q) Evaluation of the confocal signals in mTAL, cTAL, and DCT by intensity. Data are the means ± SD; * $p<0.05$ for intrastrain differences (vehicle vs. dDAVP). From ref. 82.

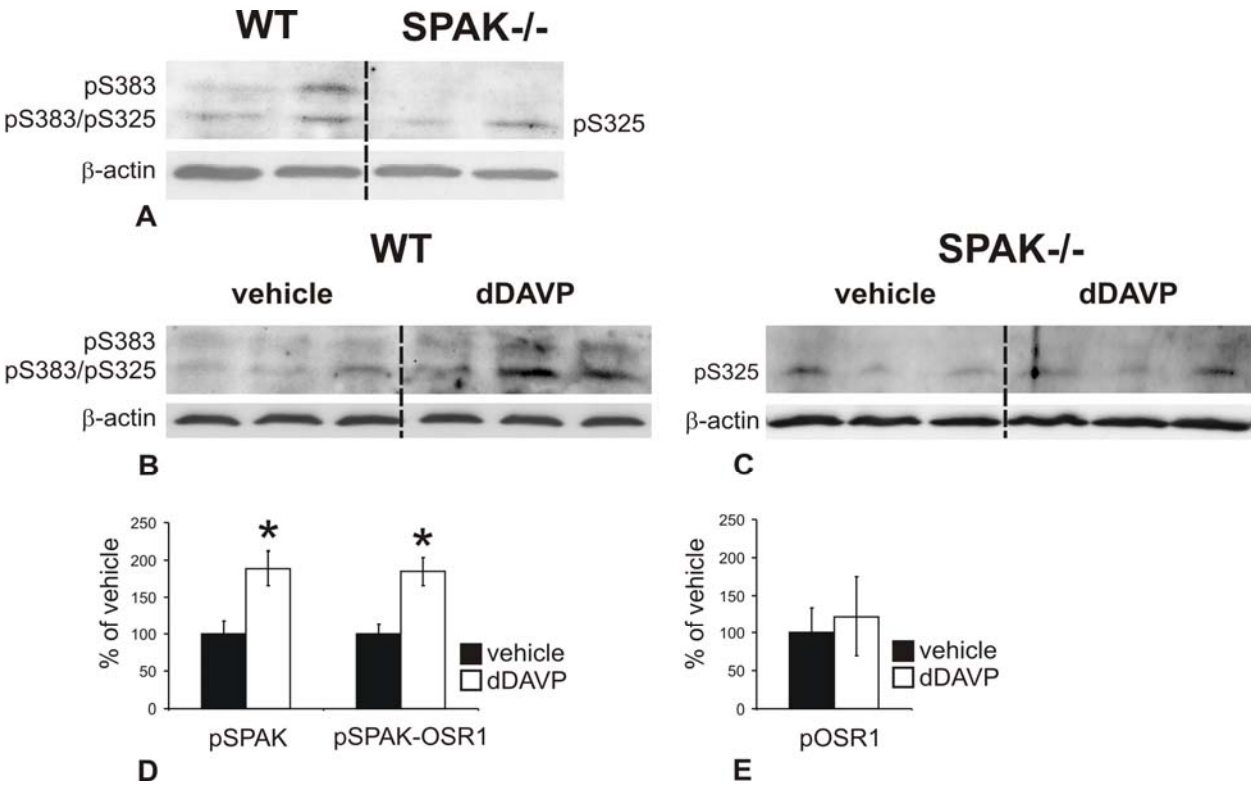

Figure 21: Acute effects of dDAVP on the phosphorylation of SPAK and OSR1 within their regulatory domains in WT and SPAK-/- kidneys, immunoblotting.

(A-C) Representative immunoblots from WT and SPAK-/- kidneys at steady state (A) and after 30 min of vehicle or dDAVP treatment (B, C) show two pS383-SPAK/pS325-OSR1 (pS383/pS325)-immunoreactive bands between 50 and 75 kDa in WT whereas in SPAK-/-, only the smaller product is clearly detectable; the larger product probably corresponds to pSPAK and the smaller, at least in part, to pOSR1; β -actin signals serve as the respective loading controls. (D, E) Densitometric evaluation of the immunoreactive signals normalized to loading controls shows increased signals in WT (+89% for the larger and +85% for the smaller products) but not in SPAK-/- kidneys upon dDAVP. Data are the means ± SD: * $p<0.05$. From ref. 82.

3.4. Role of SPAK in AVP-induced activation of NKCC2 and NCC

Next, we studied the AVP effects in SPAK knockout mice to assess the individual impact of SPAK on the activation of its downstream targets NKCC2 and NCC upon dDAVP administration.

First, we studied the effects of AVP on the surface expression and phosphorylation of NKCC2 and NCC. Quantification of immunogold signal within the apical plasma membrane of TAL cells revealed similar changes for NKCC2 surface expression in WT and SPAK-/- mice (+21% in WT and +26% SPAK-/- mice; $p<0.05$; Fig. 22 A, B, E, F, I), whereas NCC surface expression was unaffected by dDAVP in either genotype (Fig. 22 C, D, G, H, J).

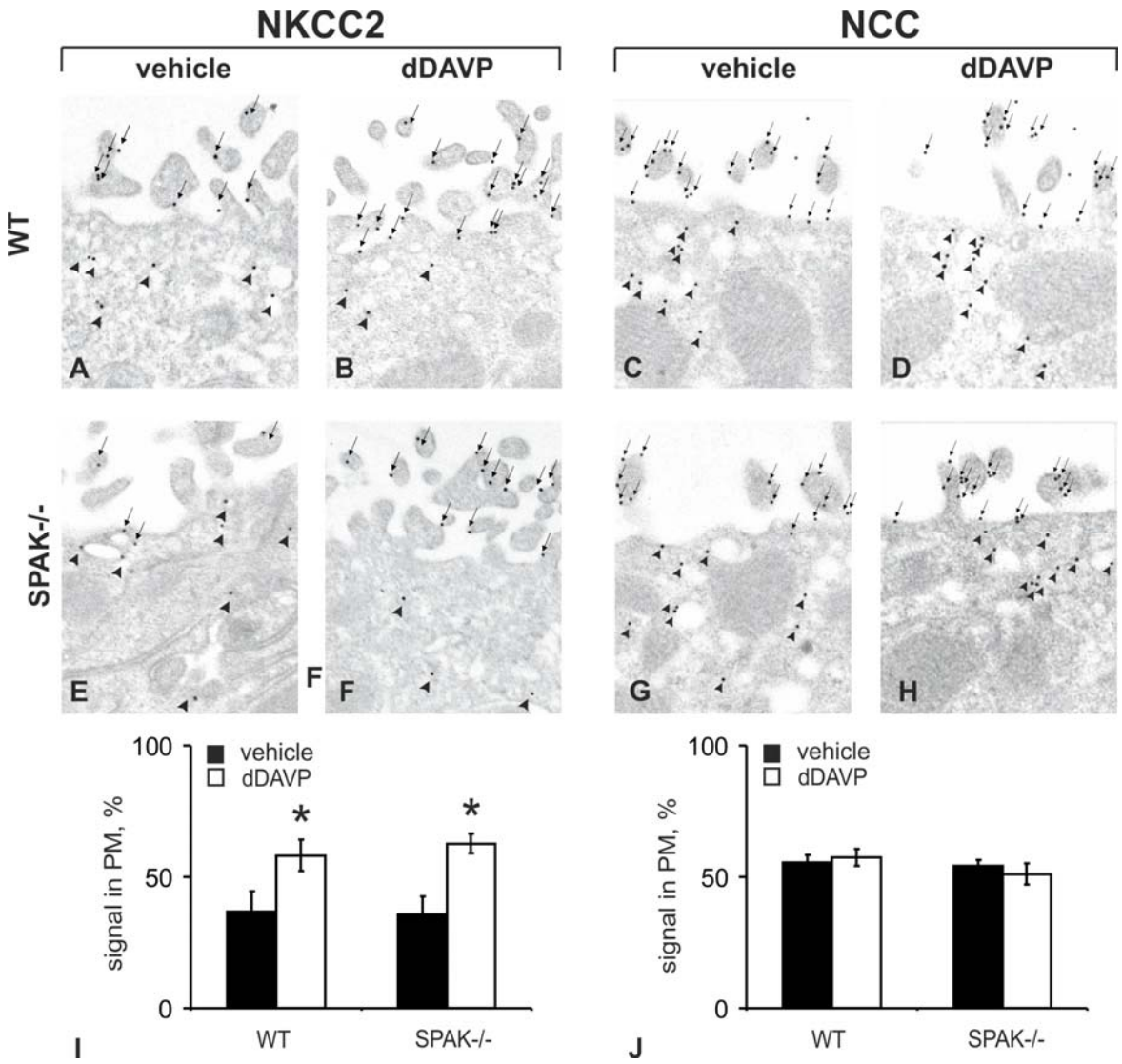

Figure 22: Acute effects of dDAVP on the luminal trafficking of NKCC2 and NCC in WT and SPAK-/- mice.

(A-F) Immunogold staining of NKCC2 in cTAL (A, B, E, F) and NCC in DCT (C, D, G, H) from WT and SPAK-/- mice after vehicle or dDAVP treatment (30 min). Transporters are distributed in the luminal plasma membrane (PM, arrows) and in cytoplasmic vesicles (arrowheads); a change is visualized for NKCC2 but not NCC (I, J). Numerical evaluations of PM NKCC2 (I) and NCC (J) signals per total of signals. Data are the means ± SD; * P<0.05. From ref. 82.

Immunoblots of NKCC2 phosphorylation at T96/T101 revealed significant increases in WT (+55%; p<0.05) and more so in SPAK -/- mice (+187%; p<0.05) upon dDAVP administration. The abundance of NKCC2 protein was concomitantly augmented in WT, but unaffected in SPAK-/- mice (Fig. 23 A-D). NCC phosphorylation was substantially increased in WT (+164% for pS71-NCC and +50% for pT58-NCC; p<0.05), but less so in SPAK-/- mice (+53% for pS71-NCC [p<0.05] and not significant for pT58-NCC; Fig. 23 A-D).

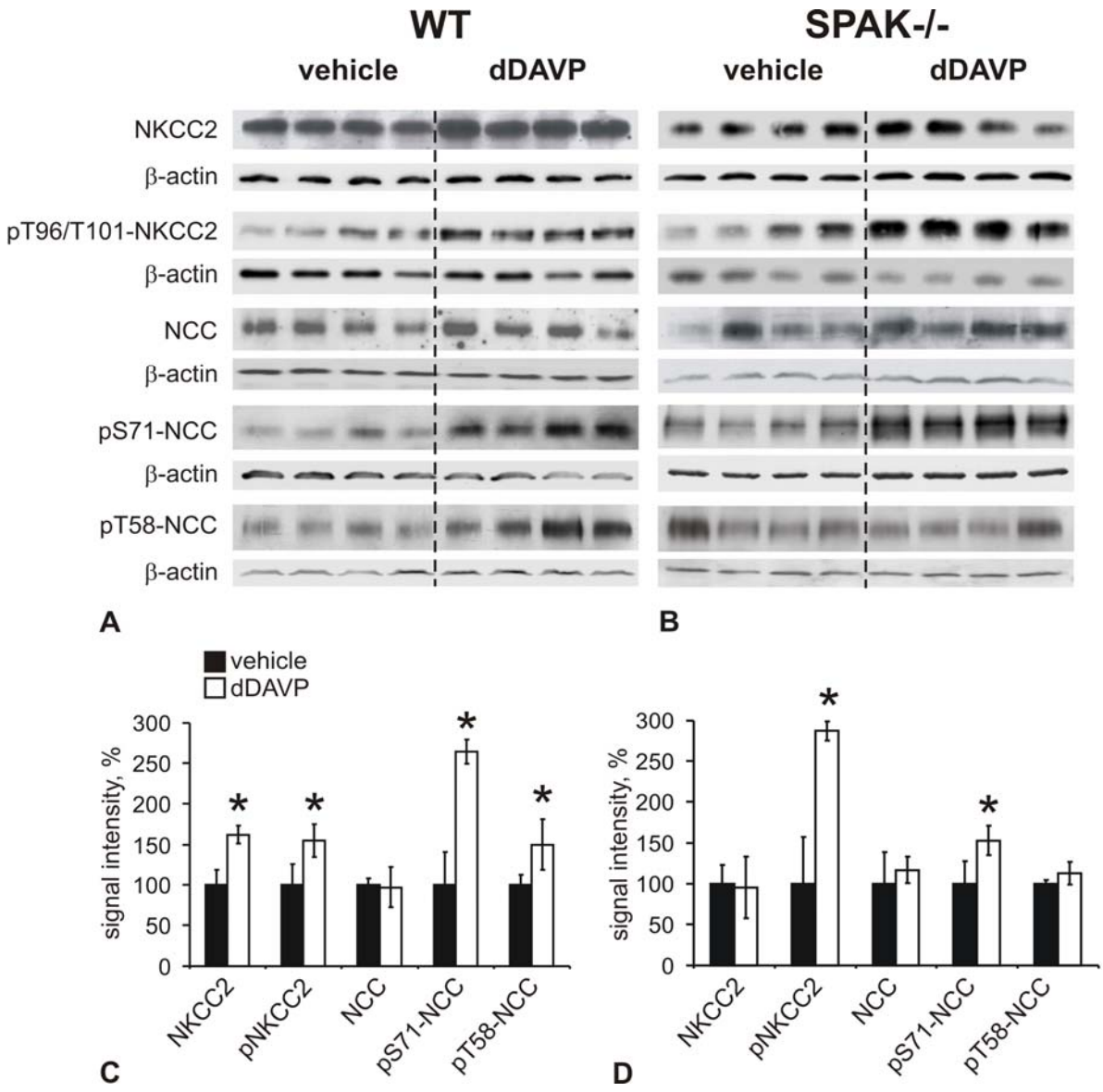

Figure 23: Acute effects of dDAVP on the abundance and phosphorylation of NKCC2 and NCC in WT and SPAK-/- mice.

Taking into account the dramatic differences in steady state phosphorylation of NKCC2 and NCC between genotypes, immunoblots from WT and SPAK-/- kidney extracts were run in parallel and the detection conditions adapted to obtain a linear range for adequate signal generation. (A, B) Representative immunoblots from WT (A) and SPAK-/- kidneys (B) after 30 min of vehicle or dDAVP treatment showing NKCC2, pT96/pT101-NKCC2, NCC, pS71-NCC, and pT58-NCC immunoreactive bands (all approximately 160 kDa); β- actin signals serve as the respective loading controls (approximately 40 kDa). (C, D) Densitometric evaluation of immunoreactive signals normalized for the loading controls. Data are the means ± SD; * $p<0.05$. From ref. 82.

These results were confirmed and extended by confocal analysis of DCT profiles including the use of an additional anti-pT53-NCC antibody (Fig. 24). Due to potential cross-reactivity of the anti-pT53-NCC antibody with pT96-NKCC2, confocal evaluation

with this antibody was preferred rather than western blot. SPAK deficiency thus had no effect on AVP-induced trafficking of NKCC2, facilitated its phosphorylation, and attenuated NCC phosphorylation.

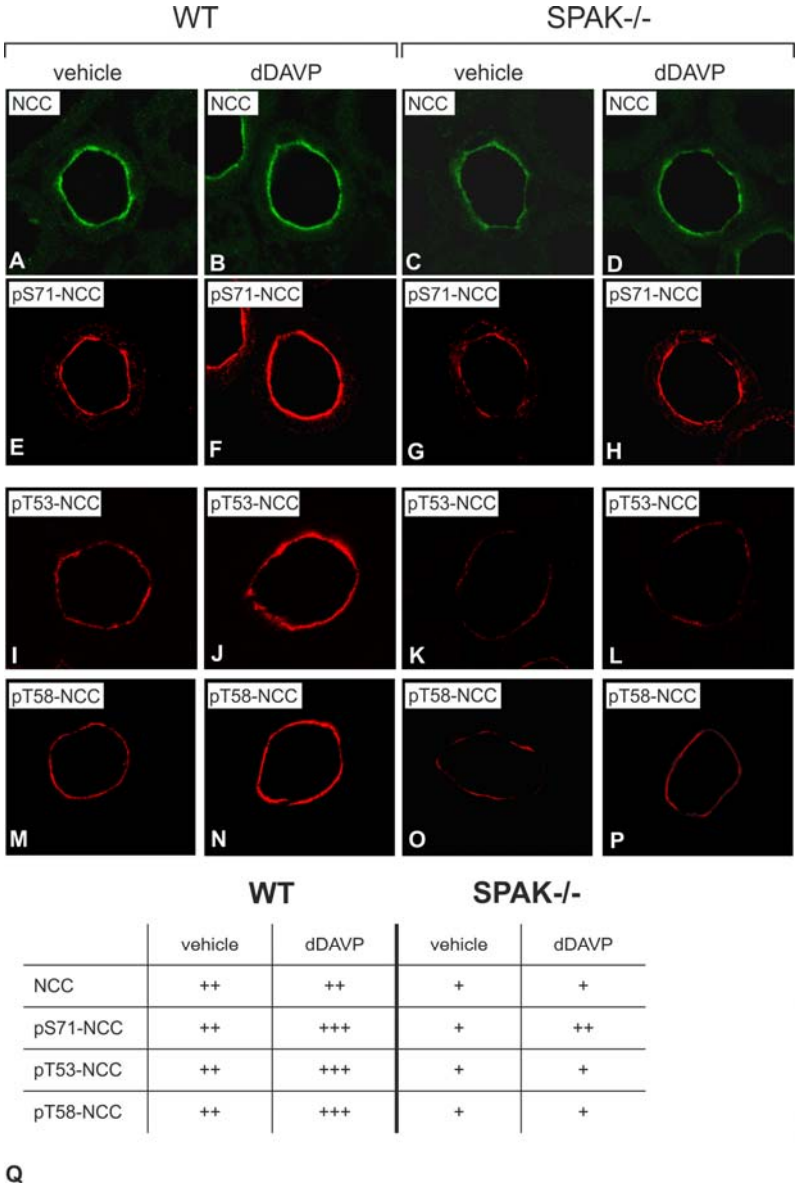

	WT		SPAK-/-	
	vehicle	dDAVP	vehicle	dDAVP
NCC	++	++	+	+
pS71-NCC	++	+++	+	++
pT53-NCC	++	+++	+	+
pT58-NCC	++	+++	+	+

Q

Figure 24: Acute effects of dDAVP on the abundance and phosphorylation of NCC, confocal evaluation.

(A-H) Representative images of DCT profiles from WT and SPAK-/- kidney sections double-stained with anti-NCC and anti-pS71-NCC antibodies after 30 min vehicle or dDAVP treatment. (E-P) Parallel confocal images of DCT profiles labeled with anti-pT53-NCC and anti-pT58-NCC antibodies (concomitant labeling of NCC was performed; not shown). (Q) Evaluation of the confocal signals by intensity. From ref. 82.

3.5. SPAK/OSR1-independent pathways are also involved in AVP-signaling

So far we have confirmed that SPAK is essential for activation of NCC, and OSR1 for activation of NKCC2. However, recent studies have also identified SPAK/OSR1-

independent NKCC2 phosphorylation at S126 (mouse NKCC2), indicating that the regulation of this transporter is still more complex. Therefore, NKCC2 phosphorylation at S126 was analyzed in WT and SPAK-/- mice after vehicle or dDAVP administration by confocal microscopy. Baseline pS126-NKCC2 signal was stronger in SPAK-/- compared to WT kidneys (+64%, p< 0.05), whereas upon dDAVP a more pronounced increase in WT than in SPAK-/- mice was registered (+118% vs. +56%, p< 0.05) which resulted in similar pS126-NKCC2 levels upon dDAVP in both genotypes (Fig. 25).

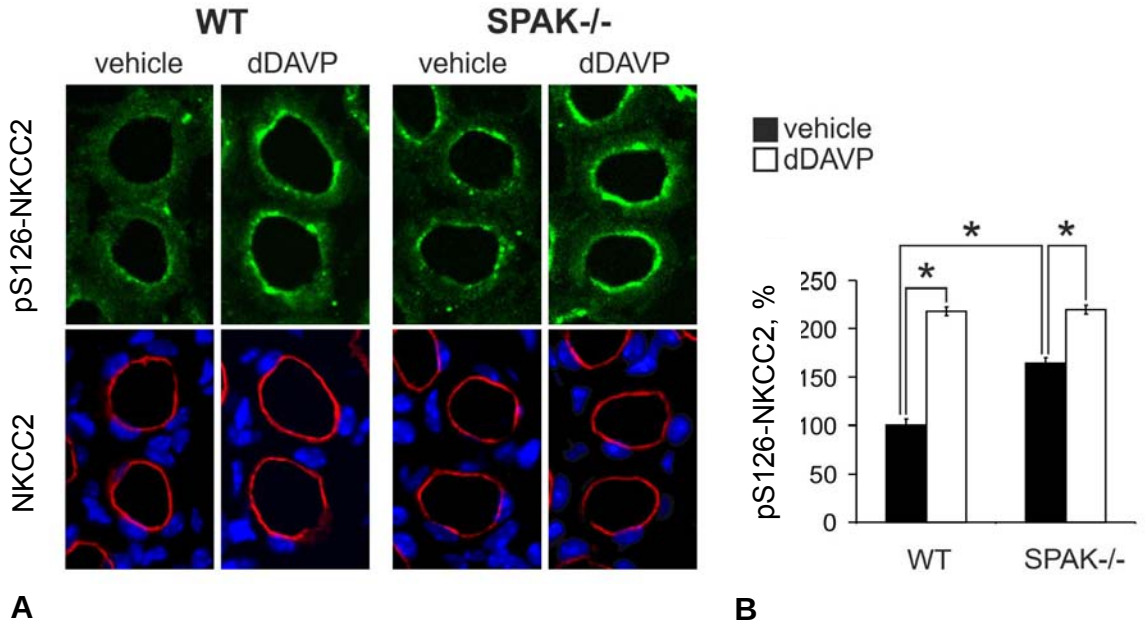

Figure 25: Acute effects of dDAVP on the phosphorylation of NKCC2 in WT and SPAK-/- mice.

Confocal characterization of medullary pS126-NKCC2 signals upon vehicle or dDAVP administration and double-staining for NKCC (A); quantitative evaluation (B). Data are the mean ± SD; * p<0.05. (n = 8 per group). Unpublished data.

Together, these results indicate that AVP induces phosphorylation of NKCC2 at both established phosphorylation targets of SPAK-OSR1 (T96/T101) as well as alternative SPAK-independent phosphoacceptor sites (S126). In contrast, AVP-induced NCC phosphorylation requires SPAK activity, particularly for the phosphorylation of conserved threonine residues.

3.6. AVP selectively modulates interactions of SPAK isoforms with NKCC2

As mentioned above, a truncated KS-SPAK isoform is abundantly expressed in TAL and may limit the phosphorylation of NKCC2 by FL-SPAK or OSR1 in a dominant-negative fashion (81). Here we tested whether AVP altered the association of activating

FL- or inhibitory KS-SPAK variants with NKCC2 using co-immunoprecipitation assays. OSR1 products were evaluated in parallel. To this end, DI rats were used owing to their well established strong response to an extrinsic AVP stimulation (36, 43).

At baseline, NKCC2 was bound to FL-SPAK more than to KS-SPAK. OSR1 isoforms interacted prominently with NKCC2, but less so with NCC (Fig. 26 A, B). Short term dDAVP significantly reduced binding of KS-SPAK (-30%, $p< 0.05$) and increased binding of FL-SPAK to NKCC2 (+62%, $p<0.05$), whereas SPAK2 and OSR1 isoforms were not affected (Fig. 26 A, C). In contrast, binding of SPAK and OSR1 isoforms to NCC was not affected by dDAVP (Fig. 26 B, D). dDAVP thus specifically modulated the interaction of NKCC2 with activating and inhibiting SPAK forms.

We evaluated whether SPAK is involved in the response of the distal nephron to long term dAVP treatment (3 days via osmotic minipumps). Physiologic effects, compared to vehicle, were more marked in WT (urine volume reduced to 25%, FENa to 23%, FEK to 26%, FECl to 47%, $p<0.05$) than in SPAK -/- mice (urine volume reduced to 38%, FENa to 57%, $p< 0.05$; Fig. 27A-E).

NKCC2 phosphorylation was raised in WT (+87%, $p<0.05$) but not in SPAK-/- which conversely showed an increase in NKCC2 abundance (+96%, $p<0.05$; Fig. 28A). NCC abundance was raised in WT (+45%, $p<0.05$) and more so in SPAK-/- mice (+201%, $p<0.05$), and NCC phosphorylation was stimulated as well in WT (+393% for pT58-NCC and +519% for pS71-NCC, $p<0.05$) and in SPAK-/- (+475% for pT58-NCC and +355% for pS71-NCC, $p<0.05$; Fig. 28A). Considering different baseline phospho-NKCC2 and phospho-NCC levels among strains, all values were normalized for the data obtained in WT mice receiving vehicle (Fig. 28 A, B). In this perspective, NKCC2, pNKCC2, and NCC abundances had reached similar levels in either genotype upon dDAVP, whereas dDAVP-induced NCC phosphorylation was selectively attenuated upon SPAK disruption at long term.

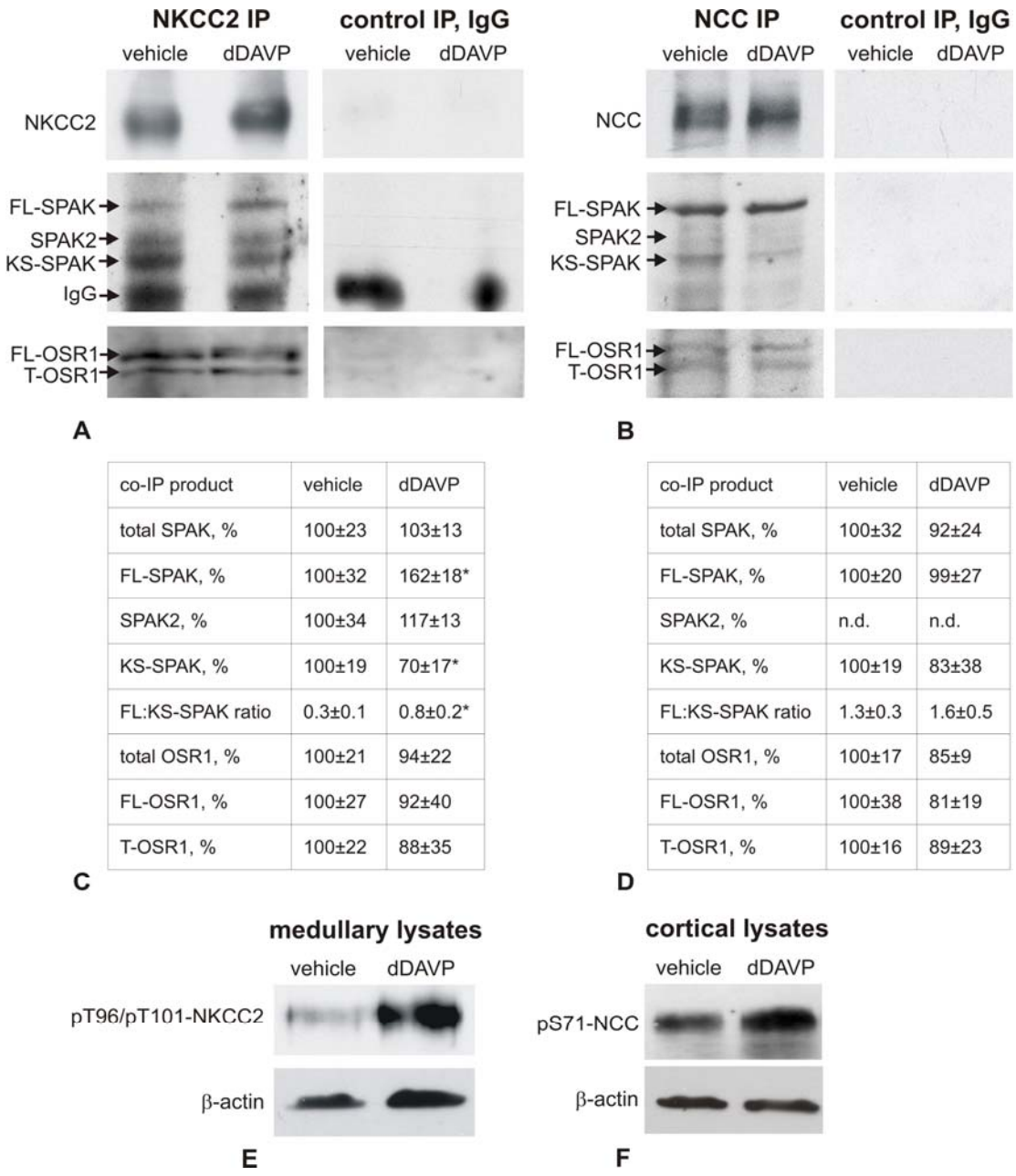

C

co-IP product	vehicle	dDAVP
total SPAK, %	100±23	103±13
FL-SPAK, %	100±32	162±18*
SPAK2, %	100±34	117±13
KS-SPAK, %	100±19	70±17*
FL:KS-SPAK ratio	0.3±0.1	0.8±0.2*
total OSR1, %	100±21	94±22
FL-OSR1, %	100±27	92±40
T-OSR1, %	100±22	88±35

D

co-IP product	vehicle	dDAVP
total SPAK, %	100±32	92±24
FL-SPAK, %	100±20	99±27
SPAK2, %	n.d.	n.d.
KS-SPAK, %	100±19	83±38
FL:KS-SPAK ratio	1.3±0.3	1.6±0.5
total OSR1, %	100±17	85±9
FL-OSR1, %	100±38	81±19
T-OSR1, %	100±16	89±23

Figure 26: Acute effects of dDAVP on binding of SPAK and OSR1 isoforms to NKCC2 and NCC in AVP-deficient Brattleboro rats with diabetes insipidus.

(A, B) Representative immunoblots of precipitates obtained after immunoprecipitation (IP) of NKCC2 from medullary (A) or NCC from cortical kidney homogenates (B) of DI rats treated with vehicle or dDAVP (30 min). NKCC2-, NCC-, C-SPAK- (FL-SPAK, SPAK2 and KS-SPAK), and OSR1-immunoreactive bands (FL- and truncated [T] OSR1 forms) are depicted. IgG bands are recognized owing to the identical host species for antibodies to NKCC2 and SPAK. Control IP with IgG was performed to exclude non-specific binding of co-immunoprecipitates. (C, D) Results of densitometric quantification of single SPAK- and OSR1 isoforms normalized to NKCC2- (C) or NCC signals (D) and evaluation of FL-SPAK:KS-SPAK ratios. Data are the means ± SD; * $p<0.05$; n.d. (not detectable) indicates no significant signal. (E, F) Effects of dDAVP stimulation were verified by parallel increases of pNKCC2 or pNCC signals in kidney extracts obtained before IP. From ref. 82.

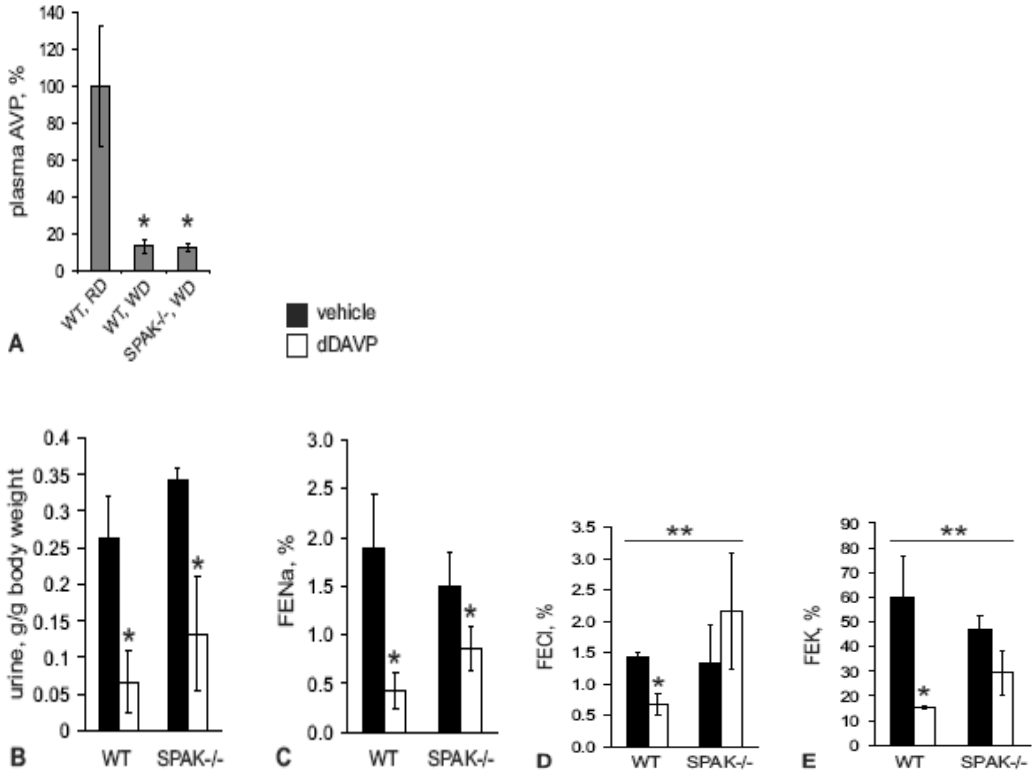

Figure 27: Long term effects of dDAVP on kidney performance in WT and SPAK-/- mice.

Water-enriched diet (food mixed with a water-containing agar; WD) administered during 3 days, before dDAVP or vehicle was given, strongly decreased endogenous plasma AVP levels in both genotypes as compared to normal AVP levels in WT mice on a regular diet (RD). (B-E) Urine volume and fractional excretion of sodium (FENa), chloride (FECl), and potassium (FEK) are shown. Two-tailed t-test was employed to analyze the intrastrain differences between vehicle and dDAVP treatments (* $p<0.05$), whereas the differences in strength of dDAVP effects between WT and SPAK-/- mice were evaluated by two-way ANOVA (** $p<0.05$). Data are the means ± SD. From ref. 82.

We next studied whether long-term dDAVP administration alters the relative abundance of SPAK and OSR1 products. dDAVP for 3 days significantly increased the abundance of FL-SPAK (+62%, $p<0.05$) and SPAK2 (+67%, $p<0.05$) in WT, whereas OSR1 isoforms were unaffected in either strain (Fig. 29 A, B). These data were verified in DI rats receiving long term dDAVP administration as well; resulting changes were similar to those obtained in WT mice (82) These results suggest a prominent role for SPAK products in distal nephron adaptation at long term.

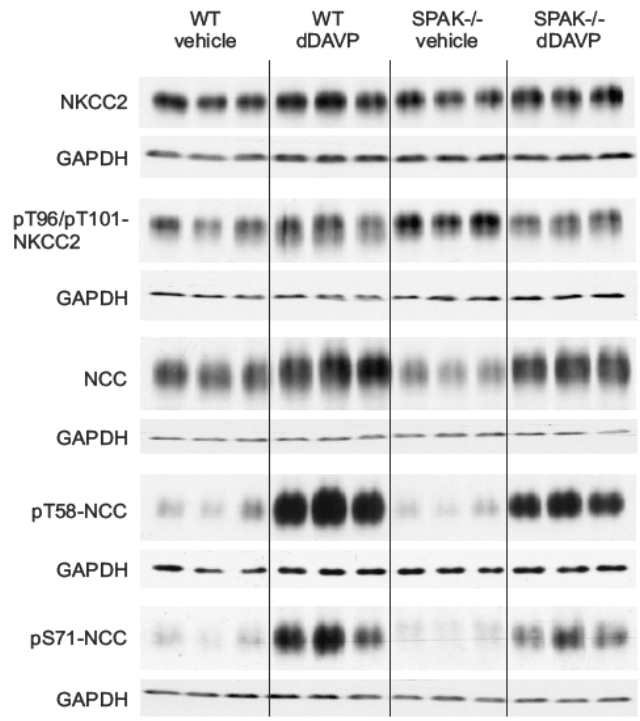

A

	WT (%)		SPAK-/- (%)	
	vehicle	dDAVP	vehicle	dDAVP
NKCC2	100±35	120±8	63±23	103±10*
pNKCC2	100±22	187±18*	228±23§	171±9
pNKCC2:NKCC2	100±56	138±23	341±110§	123±8$
NCC	100±12	145±15*	48±17§	146±25*
pT58-NCC	100±40	493±18*	42±14§	244±19*$
pT58-NCC:NCC	100±49	333±22*	90±43	171±60$
pS71-NCC	100±32	619±21*	116±35	530±34*
pS71-NCC:NCC	100±39	431±33*	249±44	369±42

B

Figure 28: Long-term effects of dDAVP on the abundance and phosphorylation of NKCC2 and NCC in WT.

(A) Representative immunoblots from WT and SPAK-/- kidneys after 3 days of vehicle or dDAVP treatment showing NKCC2, pT96/pT101-NKCC2, NCC, pS71-NCC, and pT58-NCC immunoreactive bands (all approximately 160 kDa); GAPDH signals serve as the respective loading controls (approximately 40 kDa). (B) Densitometric evaluation of immunoreactive signals normalized to loading controls and calculation of pNCC:NCC ratios. Values obtained in WT after vehicle application were set at 100%. Data are the means ± SD; * indicates $p<0.05$ for intrastrain differences (vehicle vs. dDAVP), § indicates $p<0.05$ for baseline interstrain differences (WT vs. SPAK-/- upon vehicle), and $ indicates $p<0.05$ for different responses to dDAVP in WT vs SPAK-/- genotypes as analyzed by two-way ANOVA. From ref. 82.

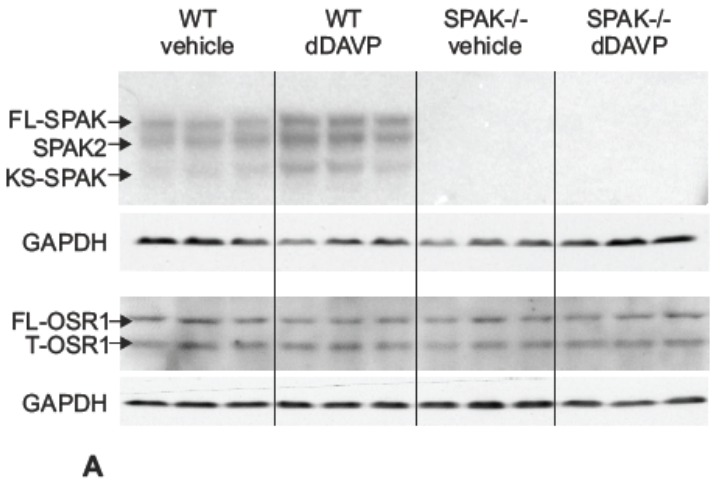

A

product	vehicle	dDAVP	vehicle	dDAVP
total SPAK	100±18	169±20*	n.d.	n.d.
FL-SPAK	100±12	162±11*	n.d.	n.d.
SPAK2	100±21	167±17*	n.d.	n.d.
KS-SPAK	100±49	275±39	n.d.	n.d.
FL:KS-SPAK	3.5±1.9	2.0±0.7	n.d	n.d
total OSR1	100±17	102±7	91±13	101±16
FL-OSR1	100±38	97±34	84±30	95±20
T-OSR1	100±5	90±9	74±18	93±4

B

Figure 29: Long term effects of dDAVP on SPAK-OSR1 in WT and SPAK-/- mice.

(A) Representative immunoblots showing SPAK and OSR1 immunoreactive bands in kidneys from WT and SPAK-/- mice after 3 days of vehicle or dDAVP treatment. GAPDH bands below the corresponding immunoblots served as loading controls. (B) Densitometric evaluation of single immunoreactive bands normalized to loading controls. Values obtained in WT after vehicle application set as 100%. Data are the means ± SD; * indicates $p<0.05$ for intrastrain differences (vehicle vs. dDAVP), n.d. (not detectable) indicates no significant signal. From ref. 82.

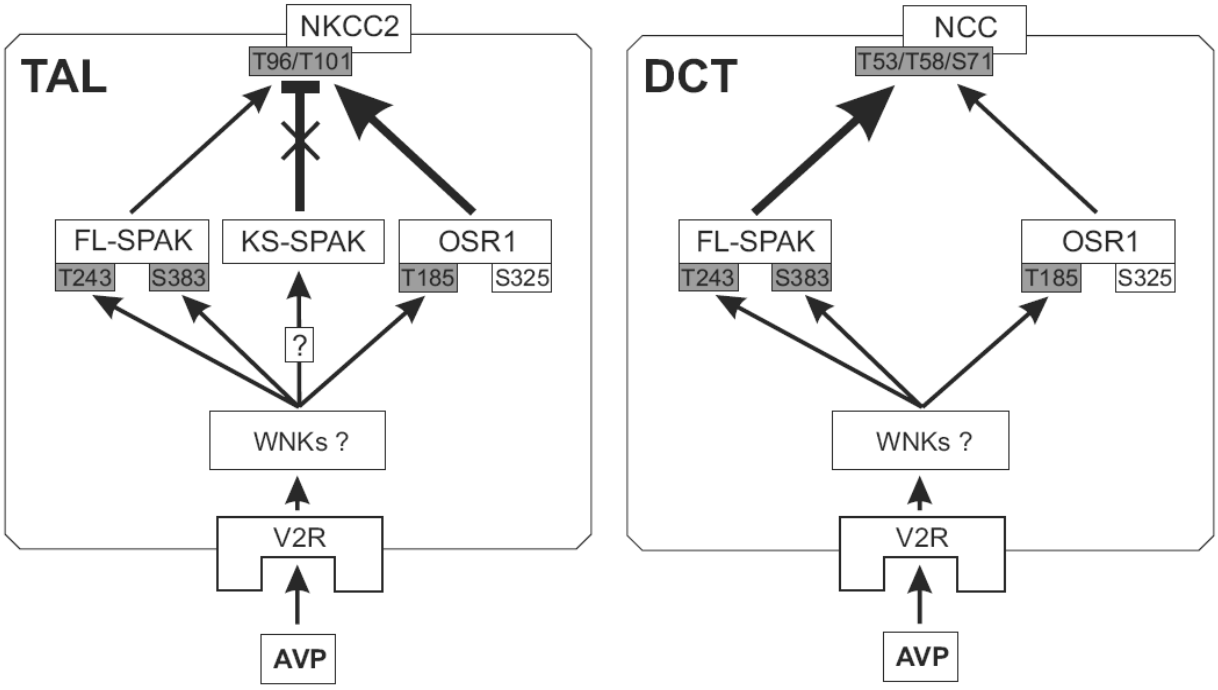

Figure 30: Proposed model of AVP-WNK-SPAK/OSR1-NKCC2/NCC signaling in the distal nephron.

Arrows indicate the downstream effects of V2R activation, the T shape indicates inhibition. The thickness of the arrows indicates the significance of the respective kinases and their actions in AVP-induced phosphorylation of NKCC2 or NCC. Boxes shaded in grey indicate phosphoacceptor sites activated by AVP signaling. In TAL, AVP attenuates the inhibitory action of KS-SPAK (cross) and facilitates the actions of FL-SPAK and OSR1. In DCT, expression of KS-SPAK is nearly absent and FL-SPAK plays the dominant role in AVP signaling. From ref. 82.

4. Discussion

4.1. Role of AVP in NCC activation

AVP facilitates NCC trafficking

The present results for the first time provide significant *in vivo* evidence for an activation of NCC in terms of its luminal trafficking and phosphorylation in response to AVP type 2 receptor agonist dDAVP. In AVP-deficient DI rats, short-term administration of dDAVP led to an increased abundance of immunoreactive NCC in the apical plasma membrane by trafficking of the cotransporter from the subapical vesicle compartment to the cell surface without concomitant changes in total NCC abundance (Fig. 8, 9). These results are similar to previous data on endocrine stimulation of NCC by Ang II (50). In contrast, no dDAVP-induced increase of NCC surface expression was noted in normal WT mice

(Figure 22). We consider that DI rats, which lack AVP from birth on, respond more intensively to external AVP administration than WT mice with an intact hormone system.

So far, it has been demonstrated in several studies (84-86) that trafficking of NCC is a major regulatory step in its activation. Clinically, NCC gene mutations in Gitelman's syndrome cause reduced surface expression, which coincides with the loss of salt (9-10). By contrast, mutations in WNK kinases found in pseudohypoaldosteronism II led to increased abundance of NCC in the surface membrane, with resulting higher salt reabsorption and hypertension (14). Thus, the trafficking of NCC to the apical membrane in response to dDAVP, as observed in this study, likely contributes to NCC activation.

AVP promotes NCC phosphorylation

We further showed that dDAVP treatment resulted in increased phosphorylation of NCC at defined amino-terminal phosphoacceptor sites (Fig. 10, 11). Phosphorylation of the amino acids T53, T58, and S71 in rat NCC has previously been established to activate the cotransporter (63, 67, 85, 87). It is, however, essential to realize that these direct effects of AVP are only part of a more complex regulatory context, and indirect effects of AVP cannot be excluded; other hormones downstream of AVP may therefore be effective. To ensure that the dDAVP-induced activation of NCC may result from the direct stimulation of V2R, we have performed studies in isolated renal tubule suspensions (50, 88). In these preparations, we observed significant phosphorylation of NCC upon dDAVP (Fig. 12). This suggests that the effect of AVP on NCC is direct and not necessarily related to the actions of other hormones.

Physiologically, the activation of NCC by AVP may serve to maximize NaCl reabsorption along the water-impermeable DCT, thus facilitating the urinary dilution and generation of the longitudinal osmotic gradient. Furthermore, antinatriuretic effects of AVP may help to maintain the circulating volume and counteract the hyponatriemic action of the hormone by balancing the increased water reabsorption.

4.2. Roles of SPAK and OSR1 for regulation of NKCC2 and NCC

Despite high homology between SPAK and OSR1 and their overlapping expression patterns along the distal nephron, these kinases affect NKCC2 and NCC differentially as

reflected by divergent phenotypes of SPAK vs. OSR1 deficiency in the kidney (56, 57). SPAK deficiency is associated with decreased function of NCC resulting in Gitelman's syndrome-like phenotype, whereas renal OSR1 deficiency leads to impaired function of NKCC2 with Bartter's syndrome-like phenotype. Additionally, increased NKCC2 phosphorylation in SPAK-/- mice was reported earlier (56). In contrast to SPAK disruption, the replacement of wild-type SPAK by a catalytically inactive mutant ($SPAK^{243A/243A}$ knockin) resulted in decreased phosphorylation of both, NKCC2 and NCC (67). We have therefore characterized renal SPAK isoforms and found an explanation for the discrepant TAL- and DCT-related phenotypes upon SPAK-deletion, and as a result, divergent effects of SPAK disruption vs. SPAK inactivation have become transparent.

SPAK is important for NCC activity

Distinct intracellular distribution of SPAK with a moderate apical signal in TAL vs. a stronger, more cytoplasmically distributed signal in DCT suggested that SPAK may have a broader function in DCT than in TAL (Fig. 13). Our data on the selectively reduced expression and phosphorylation of NCC, marked hypotrophy of DCT, together with the evidence for a dysfunction of this segment in SPAK-/- mice have confirmed the vital role of SPAK in DCT, as it had been previously suggested (81, 82).

OSR1 cannot compensate for SPAK deficiency in DCT

Although the co-expressed, homologous OSR1 showed increased abundance and redistribution to more cytoplasmic localization in DCT of SPAK-/- compared to control mice, pointing to compensatory adaptations, these adaptations were obviously not sufficient to compensate for the SPAK deficiency as shown by the present results. From a functional perspective, activity of SPAK and OSR1 depends on the phosphorylation states of their catalytic and (at least for SPAK) regulatory domains which apparently become adjusted by upstream WNK kinases (67, 70, 71). Our western blot evaluation of the respective phosphoacceptor sites revealed low phosphorylation of the kinases in the kidneys from WT and even less in SPAK-/- mice at baseline consistent with earlier data (67). This observation further indicated that compensatory activation of OSR1 had not occurred in the absence of SPAK. Confocal evaluation also demonstrated low OSR1 phosphorylation in SPAK-deficient DCT profiles, confirming that its low activity may be

linked with the failure of the kinase to compensate for SPAK deficiency at this site (Fig. 19-21).

KS- SPAK isoform inhibits NKCC2 activity

In contrast to the reduced phosphorylation of NCC we have confirmed earlier data that NKCC2 phosphorylation was drastically increased in SPAK-/- mice (56), indicating that SPAK exerts inhibitory rather than activating action in TAL. To resolve this confusing phenotype of SPAK-/- mice in TAL and DCT, we investigated SPAK isoforms in a collaborative study. In addition to the two translational variants of SPAK, described above, we have thus identified previously unrecognized, kidney-specific isoform of SPAK in mice (81). Analyzing the segmental and subcellular distribution of SPAK variants with N- and C-terminal antibodies, we identified a local predominance of the catalytically-active full-length SPAK form in DCT, whereas the truncated KS-SPAK isoform was mainly found in TAL (81). Since the kinase-deficient KS-SPAK is abundantly expressed in TAL, it may bind to NKCC2 and thereby limit the action of FL-SPAK, OSR1, and possibly also other NKCC2 activating kinases in a competitive manner. KS-SPAK in fact inhibits phosphorylation of NKCC2 in vitro (81). In the light of these observations it becomes clear why SPAK disruption and SPAK inactivation exert distinct effects on NKCC2 phosphorylation. Genetic disruption of SPAK results in the absence of all isoforms including the inhibitory KS-SPAK. Under this condition, OSR1 or other, as yet unidentified, kinases may bind to and phosphorylate NKCC2. In contrast, inactivation of SPAK by introducing a mutation ($SPAK^{243A/243A}$) in its catalytic domain, making it unresponsive to phosphorylation and activation by WNK kinases, enhances the abundance of kinase-deficient SPAK forms (KS-SPAK and inactive FL-SPAK) in TAL with resulting stronger inhibitory effects on NKCC2 (67).

KS-SPAK isoform binds NKCC2

The mechanism of the inhibitory action of kinase-deficient SPAK forms is likely the competition among the catalytically active and the inactive kinase-deficient SPAK/OSR1 variants with respect to their binding to the RFXV/I-binding motif located in the N-terminal portion of NKCC2. RFXV/I enables the transporter to directly interact with the kinases (66, 70). Even though KS-SPAK lacks the N-terminal portion including almost the entire kinase-domain, it still contains the conserved C-terminal docking site, suited

to bind to the RFXV/I motif of NKCC2. We have discovered the KS-SPAK in the rat kidney as well, where its mRNA and protein abundance was detected (Fig. 16). Our co-immunoprecipitation data have confirmed the ability of KS-SPAK to bind rat NKCC2. In fact, all known SPAK and OSR1 forms, including the inhibitory KS-SPAK, were detected as co-immunoprecipitated products after immunoprecipitation of NKCC2 from rat kidney homogenates. Our data thus describe for the first time the competitive binding of different SPAK/OSR1 forms and to downstream substrate under *in vivo* conditions.

4.3. AVP signals via SPAK and OSR1 to activate NKCC2 and NCC

NKCC2 and NCC are distributed characteristically in subapical vesicular compartments and in the plasma membrane, undergoing continued exchange in the localization due to their trafficking to and from the membrane. In spite of the reduced total abundance of NCC in SPAK-/- mice, its subcellular distribution was not different between genotypes (Fig. 22). Surface expression of NCC was not altered by dDAVP in WT or SPAK -/- mice either. In TAL, baseline surface expression and dDAVP-induced trafficking of NKCC2 were not affected by SPAK deficiency either (Fig 22). We therefore conclude that the presence of SPAK is not critical for the adequate surface expression of NKCC2 and NCC. Apart from the so recently recognized impact of OSR1 in TAL, other pathways such as cAMP/PKA signaling may probably be active as well (45, 57, 64, 73). cAMP/PKA signaling in TAL cells commonly activates NKCC2 in response to various hormones such as Ang II, parathyroid hormone, calcitonin, or glucagon. Sympathetic ß-receptor activation increases cAMP levels as well, favoring salt and water reabsorption to increase the blood pressure (89). Interestingly, contrary to the stimulatory effect of cAMP, cGMP can activate phosphodiesterase 2 (PDE2) which subsequently inhibits cAMP and NKCC2 (48). In this respect, atrial natriuretic peptides (ANP), nitric oxide (NO), or endothelin-1, released in conditions of increased blood volume, may increase cGMP levels causing salt waste due to decreased NKCC2 and NCC activity (7, 43, 90, 91).

Phosphorylation of NCC and NKCC2 is a common mechanism of their activation in response to a cascade of various stimuli such as hormones, intracellular chloride depletion (63, 92) and WNKs (70, 84-86). We have examined whether AVP modulates actions of SPAK or OSR1 to phosphorylate NKCC2 and NCC, as suggested recently (93). We observed that short term AVP-V2R stimulation increases the phosphorylation

status of SPAK/OSR1 at their homologous catalytic domain (Fig. 19). This was detected predominantly in mTAL and DCT by antibody to common epitope (anti-pT243-SPAK/pT185-OSR1), since the target sequences are identical for both kinases. A moderate increase was also detected in the absence of SPAK, suggesting limited contribution of OSR1. The response to AVP within mTAL and DCT, and not in cTAL, was possibly related with the distinct localization of upstream SPAK/OSR1 components such as the WNK 4 isoform (90). This isoform is likely to mediate AVP-induced activation of SPAK and OSR1, as previously reported for Ang II (84).

The regulatory domain (pS383-SPAK/pS325-OSR1) was activated only in WT mice, which underlines the functional heterogeneity between the kinases (Fig. 20-21). Indeed, site-directed mutagenesis studies have shown that phosphorylation of SPAK at S383 facilitates its activity by abolishing an autoinhibitory action of the regulatory domain (71), whereas no such effects were described for OSR1 (70).

Regarding NKCC2 and NCC phosphorylation, effects of dDAVP differed between WT and SPAK -/- mice (Fig. 23). The increased pNKCC2 signal in SPAK-/- was likely the result of the absence of the inhibitory KS-SPAK in TAL (81). OSR1 may effectively provide phosphorylation of NKCC2 instead of SPAK (64). On the other hand, weak OSR phosphorylation in SPAK-/- kidneys suggests that other kinases may also contribute to NKCC2 phosphorylation in response to AVP, even though OSR1 appears to be essential for basal NKCC2 phosphorylation (57, 64, 86). By contrast, NCC phosphorylation was unchanged in SPAK -/- mice upon dDAVP, indicating the predominant role of stimulatory FL-SPAK in AVP signaling in DCT (Fig. 23, 24).

Short term AVP administration mediates SPAK isoform switch

Our collaborative study revealed an intensity switch from KS-SPAK to FL-SPAK isoforms in a condition of mild intravasal volume depletion, induced by dietary sodium restriction (81). This switch may reflect physiological regulation serving to facilitate sodium reabsorption in the distal nephron in order to maintain normal arterial pressure. Possible mediators of the switch could be Ang II or AVP (41, 80, 94) but probably not aldosterone, since SPAK knockout mice displayed reduced plasma aldosterone levels in spite of stimulated renin levels. SPAK is also expressed abundantly in aldosterone-

producing adrenal glomerulosa cells, possibly reflecting impaired, SPAK-dependent aldosterone secretion in SPAK -/- mice (71). Besides diminished aldosterone plasma values, SPAK deficiency caused decreased AVP plasma levels, too. (81). SPAK is also substantially expressed in hypothalamic brain regions (95), so that its systemic deletion may interfere locally with AVP release. AVP release in turn may affect aldosterone secretion, which may further contribute to the observed low aldosterone plasma levels (96, 97). In DI rats lacking AVP, decreased aldosterone levels have been observed in spite of a stimulated RAAS as well, with the established consequences of a decreased NaCl- transport along the distal nephron (97). In SPAK -/- mice, decreased baseline phosphorylation of OSR1 and one of its substrates, NCC, were thus likely influenced by the endocrine phenotype of diminished AVP and aldosterone levels.

We further asked whether AVP, which is secreted in a state of volume depletion, induces this isoform switch as well. To this end, we examined the FL-SPAK **:** KS-SPAK ratio bound to NKCC2 in DI rats upon dDAVP. The respective co-immunoprecipitation data clearly provide *in vivo* evidence that SPAK isoforms may compete for the binding motif (RFXV/I) of NKCC2 (Fig. 26). dDAVP administration substantially modulated their interaction with NKCC2, resulting in a quantitative switch from KS-SPAK to FL-SPAK bound to NKCC2. We believe that this modulation upon AVP facilitates the activation of NKCC2. Changes in OSR1 studied in parallel were not noticeable. Our data thus show for the first time that interactions between SPAK isoforms and their substrates can be selectively modulated and that this can be induced by AVP.

Long term AVP administration increases abundance of SPAK

Besseghir et al. (98) demonstrated increased chloride reabsorption in TALs from DI rats treated several days with AVP. It is accepted that changes in NKCC2 and NCC protein abundance might account for at least some of the increases in sodium transport under chronic AVP stimulation (32). In our study, long term dDAVP decreased water and electrolyte excretion in WT and SPAK-/- mice consistent with earlier data (99) (Fig. 27). The effects of dDAVP, however, were less pronounced in SPAK-/- mice. This difference is likely to result from the reduction in NCC abundance and phosphorylation in these animals at baseline (81) (Fig. 28). The weaker NCC phosphorylation in SPAK-/- mice upon dDAVP supported this interpretation. It can be argued that a substitution with

dDAVP for only 3 days may not have been sufficient to restore the established hypotrophy of DCT in SPAK-/- mice (81). NCC abundance, however, had reached WT levels after this treatment. An attenuation of NCC phosphorylation upon SPAK disruption must therefore be noticed. On the other hand, the effects of long term dDAVP on NCC in SPAK -/- mice reveal a previously unrecognized, SPAK-independent, stimulation of NCC phosphorylation. This suggests that the increased NCC phosphorylation during chronic treatment may be an indirect response to physiological changes, as short-term dDAVP has little effect in SPAK-/- animals (see above). Given the compensatory redistribution of OSR1 in SPAK-deficient DCT and its ability to respond to AVP, we believe that OSR1 may partly mediate activation of NCC in the absence of SPAK. The changes in kinase abundances upon long term AVP substitution in mice and rats further confirm a clear dominance of SPAK over OSR1 in the respective nephron adaptations to AVP, which include a rise in abundance and activity of both cotransporters (32) (Fig. 29). Selective changes of SPAK but not OSR1 abundance have likewise been reported after long term Ang II administration (94). Although V2R-mediated effects of AVP along TAL and DCT are well established (36, 41, 62, 80), we cannot rule out potential interference of dDAVP with the RAAS in our setting (96, 97). Further studies are required to differentiate between the direct and indirect effects of AVP in the distal nephron.

AVP signals via SPAK/OSR1-independent kinase pathways to activate NKCC2

Previous studies have recently suggested that phosphorylation of NKCC2-S126 residue is important for controlling NKCC2 activity (64). Their results indicated that S126 is not controlled by SPAK or OSR1. Other work has suggested that AMPK may phosphorylate this residue (65). Our results have shown that AVP induces phosphorylation of S126-NKCC2 in a SPAK-independent manner, which confirms this data.

4.4. Perspective and Conclusion

The discovery of WNK-SPAK/OSR1-NKCC2/NCC signalling pathway along the distal nephron has extended our knowledge of renal blood pressure regulation. The present results suggest that inhibitors of SPAK, OSR1 or WNK isoforms have a potential role to act as antihypertensive agents to suppress NKCC2 and NCC activity, and thus reduce salt reabsorption. On the other hand, there are still limitations and unanswered

questions as to how WNK-SPAK/OSR1 pathway operates and is regulated: how are hormones such as angiotensin II or AVP sensed by the WNK/SPAK/OSR1 isoforms? How does phosphorylation of NKCC2 and NCC by SPAK and OSR1 stimulate their trafficking to the plasma membrane? What are the functions of translationally truncated OSR1 isoforms? Is there cross talk between the WNK-SPAK/OSR1-NKCC2/NCC pathway and other signalling networks? How may kidney-specific AMPK deficiency in mice affect NKCC2 and blood pressure? A growing body of physiologically relevant information from kidney-specific transgenic models as well as cell models deficient in specific components of the signalling pathway will permit us to resolve some of these questions in the future. Our antibodies directed against phosphorylated forms of SPAK and OSR1 cannot distinguish between the two, because the phosphorylyation sites are similar. Using other antibodies and different methods to detect the same activities may be helpful.

The results of three publications presented here, all of which were generated with a major impact of myself, provide an insight into the functioning of the AVP-WNK-SPAK/OSR1-NKCC2/NCC signaling complex along the distal nephron. For the first time, we have shown that AVP activates NCC by stimulating its luminal trafficking and phosphorylation. In SPAK-/- mice, we resolved a confusing characteristic of upregulated pNKCC2 in TAL as opposed to downregulated pNCC in DCT by identifying a novel, truncated splice SPAK variant which lacks the kinase domain, and was termed KS-SPAK for its kidney-specific expression. We have further shown that KS-SPAK is predominantly expressed in TAL where it limits the phosphorylation of NKCC2 by the full-length (FL)-SPAK or OSR1 in a dominant-negative fashion. Disruption of the SPAK gene thus abolished the inhibitory action of KS-SPAK in TAL and facilitated the phosphorylation of NKCC2 by OSR1, which has been established as a major NKCC2-activating kinase. Unlike KS-SPAK, FL-SPAK was chiefly expressed in DCT and appears to be crucial for NCC phosphorylation. Our results show an essential role for SPAK in acute AVP signaling to NCC in the DCT. Interestingly, however, compensatory processes occur during chronic V2R stimulation, which may permit AVP to stimulate NCC in a SPAK-independent manner. In contrast to the effects along DCT, SPAK deletion, which increases basal NKCC2 phosphorylation along the TAL, leads to an enhanced dDAVP effect on NKCC2 in the short-term. As shown diagrammatically in

Figure 30, the dominant inhibitory KS-SPAK and the stimulatory FL-SPAK variants were modulated differentially in response to AVP to selectively bind and control the activation of NKCC2, whereas the phosphorylation of NCC was chiefly governed by FL-SPAK. By contrast, OSR1 appeared to exert predominantly baseline functions, mainly in TAL, where its activity may be highly dependent on KS-SPAK abundance. Our data thus identify SPAK as a crucial kinase that differentially regulates Na+ reabsorption in the renal cortex and medulla under the endocrine control of AVP. The findings in part represent the complex interaction of hormones, kinases and transporter in TAL and DCT, permitting mammals to balance their salt and water homeostasis and thus their arterial blood pressure.

References

1. World Health Organisation: Global health risks: mortality and burden of disease attributable to selected major risks, 2009. (Accessed May 08, 2012, at http://www.who.int/healthinfo/global_burden_disease/GlobalHealthRisks_report_full.pdf).

2. World Health Organisation: The prevalence of raised blood pressure- Situation and trends, 2011. (Accessed December 17, 2011, at http://www.who.int/gho/ncd/risk_factors/blood_pressure_prevalence_text/en/index.html).

3. Meneton P, Jeunemaitre X, de Wardener HE, MacGregor GA. Links between salt intake, renal salt handling, blood pressure, and cardiovascular disease. Physiol Rev 2005;85:679-715.

4. Strazzullo P, D'Elia L, Kandala NB, Cappuccio FB. Salt intake, stroke, and cardiovascular disease: Meta-analysis of prospective studies. BMJ 2009;339:b4567.

5. Guyton AC. Blood pressure control- special role of the kidneys and body fluids. Science 1991;17:1011-1053.

6. O'Shaughnessy KM, Karet FE. Salt handling and hypertension. Annu.Rev. Nutr. 2006;26:343-365.

7. Gamba G. Molecular physiology and pathophysiology of electroneutral cationchloride cotransporters. Physiol. Rev. 2005;85:423-493.

8. Piechotta K, Lu J, Delpire E. Cation chloride cotransporters interact with the stress-related kinases Ste20-related proline-alanine-rich kinase (SPAK) and oxidative stress response 1 (OSR1). J. Biol. Chem. 2002;277:50812-50819.

9. Simon DB, Karet FE, Hamdan JM, DiPietro A, Sanjad SA, Lifton RP. Bartter's syndrome, hypokalaemic alkalosis with hypercalciuria, is caused by mutations in the Na-K-2Cl cotransporter NKCC2. Nat. Genet. 1996;13:183-188.

10. Simon DB, Nelson-Williams C, Bia MJ, et al. Gitelman's variant of Bartter's syndrome, inherited hypokalaemic alkalosis, is caused by mutations in the thiazide-sensitive Na-Cl cotransporter. Nat. Genet. 1996;12:24-30.

11. Lang F, Capasso G, Schwab M, Waldegger S. Renal tubular transport and the genetic basis of hypertensive disease. Clin Exp Nephrol 2005;9 (2):91-99.

12. Capasso G, Rizzo M, Evangelista C, et al. Altered expression of renal apical plasma membrane Naþ transporters in the early phase of genetic hypertension. Am J Physiol Renal Physiol 2005;288 (6):F1173-F1182.

13. Capasso G, Cantone A, Evangelista C, et al. Channels, carriers, and pumps in the pathogenesis of sodium-sensitive hypertension. Semin Nephrol 2005;25 (6):419-424.

14. Wilson FH, Disse-Nicodème S, Choate KA, Human hypertension caused by mutations in WNK kinases. Science 2001;293(5532):1107-12.

15. Lang F. Transportprozesse in der Henle-Schleife und Harnkonzentrierung. In: Lang F, Thews G, eds. Physiologie des Menschen mit Pathophysiologie. 31st ed. Heidelberg, Germany: Springer- Lehrbuch, 2011;VII:629-663.

16. Greger R. Physiology of renal sodium transport. Am J Med Sci. 2000;319(1):51-62.

17. Kriz W. The architectonic and functional structure of the rat kidney. Z Zellforsch Mikrosk Anat. 1967;82(4):495-535.

18. Glover M, Zuber AM, O'Shaughnessy KM. Hypertension, Dietary salt intake, and the role of the thiazide-sensitive sodium chloride transporter NCCT. Cardiovasc Ther. 2011;29(1):68-76.

19. Bobulescu IA, Moe OW. Luminal Na(+)/H(+) exchange in the proximal tubule. Pflugers Arch 2009;458:5-2.

20. Bachmann S, Bostanjoglo M, Schmitt R, Ellison DH. Sodium transport-related proteins in the mammalian distal nephron - distribution, ontogeny and functional aspects. Anat Embryol (Berl). 1999;200(5):447-68.

21. Pallone TL, Turner MR, Edwards A, Jamison RL. Countercurrent exchange in the renal medulla. Am J Physiol Regul Integr Comp Physiol. 2003;284(5):R1153-75.

22. Barbry P, Hofman P. Molecular biology of Na1 absorption. Am. J. Physiol 1997; 273:G571-G585.

23. Grantham JJ, Burg MB. Effect of vasopressin and cAMP on permeability of isolated collecting tubules. Am J Physiol 1966;211:255-259.

24. Inoue T, Nonoguchi H, Tomita K. Physiological effects of vasopressin and atrial natriuretic peptide in the collecting duct. Cardiovasc Res 2001;5:470-480.

25. Nishimoto G, Zelenina M, Li D, et al. Arginine vasopressin stimulates phosphorylation of aquaporin-2 in rat renal tissue. Am J Physiol Renal Physiol 1999;276:F254-F259.

26. Gamba G. The nanopeptide hormone vasopressin is a new player in the modulation of renal Na^+– Cl^- cotransporter activity. Kidney Int 2010;78:127-129.

27. Bankir L. Antidiuretic action of vasopressin: quantitative aspects and interaction between V1a and V2 receptor mediated effects. Cardiovasc Res 2001;51:372-390.

28. Maybauer MO, Maybauer DM, Enkhbaatar P, et al. Physiology of vasopressin receptors. Best Pract Res Clin Anaesthesiol 2008;22:253-263.

29. Leaf A, Bartter FC, Santos RF, et al. Evidence in man that urinary electrolyte loss induced by pitressin is a function of water retention. J Clin Invest 1953;32:868-878.

30. Michimata M, Mizukami K, Suzuki M, et al. Vasopressin-independent renal urinary concentration: increased rBSC1 and enhanced countercurrent multiplication. Kidney Int 2003;64:933-938.

31. Lolait SJ, O'Carroll AM, McBride OW, Konig M, Morel A, Brownstein MJ. Cloning and characterization of a vasopressin V2 receptor and possible link to nephrogenic diabetes insipidus. Nature 1992;357:336-339.

32. Ecelbarger CA, Kim GH, Wade JB, Knepper MA. Regulation of the abundance of renal sodium transporters and channels by vasopressin. Exp Neurol 2001;171:227-234.

33. Serradeil-Le Gal C, Wagnon J, Valette G, et al. Nonpeptide vasopressin receptor antagonists: development of selective and orally active V_{1a}, V_2 and V_{1b} receptor ligands. Prog Brain Res 2002;139:197-210.

34. Sands JM, Layton HE. The physiology of urinary concentration: an update. Semin Nephrol 2009;29:178-195.

35. Fenton RA. Essential role of vasopressin-regulated urea transport processes in the mammalian kidney. Pflugers Arch 2009;458:169-177.

36. Mutig K, Paliege A, Kahl T, Jöns T, Müller-Esterl W, Bachmann S. Vasopressin V2 receptor expression along rat, mouse, and human renal epithelia with focus on TAL. Am J Physiol Renal Physiol 2007;293:F1166-F1177.

37. Ostrowski NL, Young WS 3rd, Knepper MA, Lolait SJ. Expression of vasopressin V1a and V2 receptor messenger ribonucleic acid in the liver and kidney of embryonic, developing, and adult rats. Endocrinology 1993;133(4):1849-59.

38. Bankir L, Bichet DG, Bouby N. Vasopressin V2 receptors, ENaC, and sodium reabsorption: a risk factor for hypertension? Am J Physiol Renal Physiol 2010;299:F917-F928.

39. Schafer JA, Hawk CT. Regulation of Na+ Channels in the cortical collecting duct by AVP and mineralocorticoids. Kidney Int 1992;41:255-268

40. Hebert SC, Andreoli TE. Control of NaCl transport in the thick ascending limb. Am J Physiol Renal Fluid Electrolyte Physiol 1984;246:F745-F756.

41. Welker P, Böhlick A, Mutig K, et al. Renal Na-K-Cl cotransporter activity and vasopressin-induced trafficking are lipid raftdependent. Am J Physiol Renal Physiol 2008;295:F559-F567.

42. Ecelbarger CA, Knepper MA, Verbalis JG. Increased abundance of distal sodium transporters in rat kidney during vasopressin escape. J Am Soc Nephrol. 2001;12(2):207-17.

43. Gimenez I, Forbush B. Short-term stimulation of the renal Na-K-Cl cotransporter (NKCC2) by vasopressin involves phosphorylation and membrane translocation of the protein. J Biol Chem 2003;278:26946-16951.

44. Luft FC. Vasopressin, urine concentration, and hypertension: a new perspective on an old story. Clin J Am Soc Nephrol. 2007 Mar;2(2):196-7.

45. Ares GR, Caceres PS, Ortiz PA. Molecular regulation of NKCC2 in the thick ascending limb. Am J Physiol Renal Physiol. 2011;301(6):F1143-59.

46. Ortiz PA. cAMP increases surface expression of NKCC2 in rat thick ascending limbs: role of VAMP. Am J Physiol Renal Physiol. 2006;290(3):F608-16.

47. Caceres PS, Ares GR, Ortiz PA. cAMP stimulates apical exocytosis of the renal Na(+)-K(+)-2Cl(-) cotransporter NKCC2 in the thick ascending limb: role of protein kinase A. J Biol Chem. 2009;284(37):24965-71.

48. Ares GR, Caceres P, Alvarez- Leefmans FJ, Ortiz PA. cCMP decreases surface NKCC2 levels in the thick ascending limb: role of phosphodiesterase 2 (PDE2). Am J Physiol Renal Physiol 2008;295:F8877-F887.

49. Dimke H. Exploring the intricate regulatory network controlling the thiazide-sensitive NaCl cotransporter (NCC). Pflugers Arch. 2011;462(6):767-77.

50. Sandberg MB, Riquier AD, Pihakaski- Maunsbach K, McDonough AA, Maunsbach AB. AngII provokes acute trafficking of distal Na+, Cl- cotransporter to apical membrane. Am J Physiol Renal Physiol 2007;293:F662-F669.

51. McCormick JA, Ellison DH. The WNKs: atypical protein kinases with pleiotropic actions. Physiol Rev. 2011;91(1):177-219. Review.

52. Hoorn EJ, Nelson JH, McCormick JA, Ellison DH. The WNK kinase network regulating sodium, potassium, and blood pressure. J Am Soc Nephrol. 2011;22(4):605-14. Review.

53. Chiga M, Rafiqi FH, Alessi DR, et al. Phenotypes of pseudohypoaldosteronism type II caused by the WNK4 D561A missense mutation are dependent on the WNK-OSR1/SPAK kinase cascade. J Cell Sci. 2011;124(Pt 9):1391-5.

54. Zhou B, Zhuang J, Gu D, et al. WNK4 enhances the degradation of NCC through a sortilin-mediated lysosomal pathway. J Am Soc Nephrol. 2010;21(1):82-92.

55. Subramanya AR, Liu J, Ellison DH, Wade JB, Welling PA. WNK4 diverts the thiazide-sensitive NaCl cotransporter to the lysosome and stimulates AP-3 interaction. J Biol Chem. 2009 3;284(27):18471-80.

56. Yang SS, Lo YF, Wu CC, et al. SPAK knockout mice manifest Gitelman syndrome and impaired vasoconstriction. J Am Soc Nephrol 2010; 21:1868-1877.

57. Lin SH, Yu IS, Jiang ST, et al. Impaired phosphorylation of Na+-K+-2Cl- cotransporter by oxidative stress-responsive kinase-1 deficiency manifests hypotension and Bartter-like syndrome. Proc Natl Acad Sci USA 2011;108(42):17538-43.

58. Uchida S. Pathophysiological roles of WNK kinases in the kidney. Pflugers Arch. 2010;460(4):695-702.

59. Yang CL, Angell J, Mitchell R, Ellison DH. WNK kinases regulate thiazide-sensitive Na-Cl cotransport. J Clin Invest. 2003;111(7):1039-45.

60. Lalioti MD, Zhang J, Volkman HM, et al. Wnk4 controls blood pressure and potassium homeostasis via regulation of mass and activity of the distal convoluted tubule. Nat Genet. 2006;38(10):1124-32.

61. Yang SS, Morimoto T, Rai T, et al. Molecular pathogenesis of pseudohypoaldosteronism type II: generation and analysis of a Wnk4(D561A/+) knockin mouse model. Cell Metab. 2007;5(5):331-44.

62. Giménez I, Forbush B. Regulatory phosphorylation sites in the NH2 terminus of the renal Na-K-Cl cotransporter (NKCC2). Am J Physiol Renal Physiol. 2005;289(6):F1341-5.

63. Pacheco-Alvarez D, Cristóbal PS, Meade P, et al. The Na+ Cl- cotransporter is activated and phosphorylated at the amino-terminal domain upon intracellular chloride depletion. J Biol Chem 2003;281:28755-28763.

64. Richardson C, Sakamoto K, de los Heros P, et al. Regulation of the NKCC2 ion cotransporter by SPAK-OSR1-dependent and -independent pathways. J Cell Sci. 2011;124(Pt 5):789-800.

65. Fraser SA, Gimenez I, Cook N, Jennings I, Katerelos M, Katsis F. Regulation of the renal specific Na+-K+-2Cl- co-transporter NKCC2 by AMP-activated protein kinase (AMPK). Biochem J 2007;405:85-93.

66. Richardson C, Alessi DR. The regulation of salt transport and blood pressure by the WNK-SPAK/OSR1 signalling pathway. J Cell Sci 2008;121:3293-3304.

67. Richardson C, Rafiqi FH, Karlsson HK, et al. Activation of the thiazide-sensitive Na+-Cl- cotransporter by the WNK-regulated kinases SPAK and OSR1. J Cell Sci. 2008;121(Pt 5):675-84.

68. Lin SH, Shiang JC, Huang CC, Yang SS, Hsu YJ, Cheng CJ. Phenotype and genotype analysis in Chinese patients with Gitelman's syndrome. J Clin Endocrinol Metab. 2005;90(5):2500-7.

69. Vitari AC, Deak M, Morrice NA, Alessi DR. The WNK1 and WNK4 protein kinases that are mutated in Gordon’s hypertension syndrome phosphorylate and activate SPAK and OSR1 protein kinases. Biochem J. 2005;391(Pt 1):17-24.

70. Vitari AC, Thastrup J, Rafiqi FH, et al. Functional interactions of the SPAK/OSR1 kinases with their upstream activator WNK1 and downstream substrate NKCC1. Biochem J 2006;397:223-231.

71. Delpire E, Gagnon KB. SPAK and OSR1: STE20 kinases involved in the regulation of ion homoeostasis and volume control in mammalian cells. Biochem J 2008.409:321–331.

72. Johnston AM, Naselli G, Gonez LJ, Martin RM, Harrison LC, Deaizpurua JH. SPAK, a STE20/SPS1-related kinase that activates the p38 pathway. Oncogene 2000;19:4290-4297.

73. Rafiqi FH, Zuber AM, Glover M, Role of the WNK-activated SPAK kinase in regulating blood pressure. EMBO Mol Med. 2010;2(2):63-75.

74. Dowd BF, Forbush B. PASK (proline-alanine-rich STE20-related kinase), a regulatory kinase on Na-K-Cl cotransporter (NKCC1). J. Biol. Chem. 2003;278:27347-27353.

75. Rodan AR, Huang CL. An emerging role for SPAK in NCC, NKCC, and blood pressure regulation. J Am Soc Nephrol. 2010;21(11):1812-4.

76. Wang Y, O'Conenell JR, McArdle PF, et al. From the cover: Whole-genome association study identifies STK39 as a hypertension susceptibility gene. Proc Natl Acad Sci USA 2009;1006:226-231.

77. Reiche J, Theilig F, Rafiqi FH, et al.. SORLA/SORL1 functionally interacts with SPAK to control renal activation of Na(+)-K(+)-Cl(-) cotransporter 2. Mol Cell Biol. 2010;30(12):3027-37.

78. Mutig K, Kahl T, Saritas T, et al. Activation of the bumetanide-sensitive Na+,K+,2Cl- cotransporter (NKCC2) is facilitated by Tamm-Horsfall protein in a chloride-sensitive manner. J Biol Chem. 2011 26;286(34):30200-10.

79. Gunaratne R, Braucht DW, Rinschen MM, et al. Quantitative phosphoproteomic analysis reveals cAMP/vasopressin-dependent signaling pathways in native renal thick ascending limb cells. Proc Natl Acad Sci U S A. 2010;107(35):15653-8.

80. Mutig K, Saritas T, Uchida S, et al. Short-term stimulation of the thiazide-sensitive Na+-Cl- cotransporter by vasopressin involves phosphorylation and membrane translocation. Am J Physiol Renal Physiol. 2010;298(3):F502-9.

81. McCormick JA, Mutig K, Nelson JH, et al. A SPAK isoform switch modulates renal salt transport and blood pressure. Cell Metabolism 2011;14:352-364.

82. Saritas T, Borschewski A, McCormick JA, et al. SPAK differentially mediates vasopressin effects on sodium cotransporters. J Am Soc Nephrol. 2013;24(3):407-18.

83. Subramanya AR, Yang CL, Zhu X, Ellison DH. Dominant-negative regulation of WNK1 by its kidney-specific kinase-defective isoform. Am J Physiol Renal Physiol. 2006;290(3):F619-24.

84. San-Cristobal P, Pacheco-Alvarez D, Richardson C, et al. Angiotensin II signaling increases activity of the renal Na-Cl cotransporter through a WNK4-SPAK-dependent pathway. Proc Natl Acad Sci U S A. 2009;106(11):4384-9

85. Chiga M, Rai T, Yang SS, et al. Dietary salt regulates the phosphorylation of OSR1/SPAK kinases and the sodium chloride cotransporter through aldosterone. Kidney Int 2008;74:1403–1409

86. Rinehart J, Kahle KT, de Los Heros P, et al. WNK3 kinase is a positive regulator of NKCC2 and NCC, renal cation-Cl- cotransporters required for normal blood pressure homeostasis. Proc Natl Acad Sci U S A. 2005;102(46):16777-82.

87. Vallon V, Schroth J, Lang F, Kuhl D, Uchida S. Expression and phosphorylation of the Na-Cl.cotransporter NCC in vivo is regulated by dietary salt, potassium and SGK1. Am J Physiol Renal Physiol 2009;297:F704-F712.

88. Kim GH, Masilamani S, Turner R, Mitchell C, Wade JB, Knepper MA. The thiazide-sensitive Na-Cl cotransporter is an aldosterone-induced protein. Proc Natl Acad Sci USA 1998;95:14552–14557.

89. Berrera M, Dodoni G, Monterisi S, Pertegato V, Zamparo I, Zaccolo M. A toolkit for real-time detection of cAMP: insights into compartmentalized signaling. Handb Exp Pharmacol 2008;186:285-298.

90. Ohno M, Uchida K, Ohashi T, et al. Immunolocalization of WNK4 in mouse kidney. Histochem Cell Biol. 2011;136(1):25-35.

91. Bailly C. Effect of luminal atrial natriuretic peptide on chloride reabsorption in mouse cortical thick ascending limb: inhibition of endothelin. J Am Soc Nephrol 2000;11:1791-1797.

92. Ponce-Coria J, San-Cristobal P, Kahle KT, et al. Regulation of NKCC2 by a chloride-sensing mechanism involving the WNK3 and SPAK kinases. Proc Natl Acad Sci U S A. 2008;105(24):8458-63.

93. Pedersen NB, Hofmeister MV, Rosenbaek LL, Nielsen J, Fenton RA.Vasopressin induces phosphorylation of the thiazide-sensitive sodium chloride cotransporter in the distal convoluted tubule.Kidney Int. 2010;78(2):160-9.

94. van der Lubbe N, Lim CH, Fenton RA. Angiotensin II induces phosphorylation of the thiazide-sensitive sodium chloride cotransporter independent of aldosterone. Kidney Int. 2011;79(1):66-76.

95. Piechotta K, Garbarini N, England R, Delpire E. Characterization of the interaction of the stress kinase SPAK with the Na+-K+-2Cl- cotransporter in the nervous system: evidence for a scaffolding role of the kinase. J Biol Chem. 2003;278(52):52848-56.

96. Möhring J, Kohrs G, Möhring B, Petri M, Homsy E, Haack D. Effects of prolonged vasopressin treatment in Brattleboro rats with diabetes insipidus. Am J Physiol. 1978;234(2):F106-11.

97. Mazzocchi G, Malendowicz LK, Rocco S, Musajo F, Nussdorfer GG. Arginine-vasopressin release mediates the aldosterone secretagogue effect of neurotensin in rats. Neuropeptides. 1993;24(2):105-8.

98. Besseghir, K., Trimble ME, and Stoner L. Action of ADH on isolated medullary thick ascending limb of the Brattleboro rat. Am. J. Physiol 1986;251(2 Pt 2): F271–277.

99. Perucca J, Bichet DG, Bardoux P, Bouby N, Bankir L. Sodium excretion in response to vasopressin and selective vasopressin receptor antagonists. J Am Soc Nephrol. 2008;19(9):1721-31.

5. Acknowledgements

Das Ausmaß dieser Promotionsarbeit wäre ohne die Unterstützung vieler Menschen nicht möglich gewesen. Mein Dank gilt vor allem meiner Familie und Theresa, die mich stets durch ihr uneingeschränktes Vertrauen und ihre moralische Hilfe bestärkt haben.
Ebenso danke ich meinem Betreuer Dr. Kerim Mutig, der mir die experimentelle Forschung Schritt für Schritt näher gebracht hat sowie bei Thomas, Alex und den technischen Assistenten die mir hilfsbereit bei experimentellen oder inhaltlichen Fragen zur Seite standen.
Danken möchte ich allen anderen Mitarbeitern der AG Bachmann, insbesondere Tom und Saskia, die mir durch ihren Humor auch in schwierigen Laborzeiten die Arbeit annehmbar machten.

I'd like to thank Jim, Joshua and Shaunessy for the fun and all the help in the lab. I'd like to thank Dr. Ellison who allowed me to gain experiences in his laboratory.

Ich bedanke mich bei der Studienstiftung des deutschen Volkes für ihre finanzielle und ideelle Unterstützung.

Schließlich möchte ich mich besonders bei Herrn Prof. Bachmann für seine Betreuung bei der Fertigstellung der verschiedenen Manuskripte und der Dissertation bedanken. Er ermöglichte mir in die Forschung einzusteigen und meine Ergebnisse vor internationalem Fachpublikum zu präsentieren. Prof. Bachmann hat meine personelle Entwicklung maßgeblich geprägt.

Publikationen:

Short-term stimulation of the thiazide-sensitive Na+,Cl cotransporter by vasopressin involves phosphorylation and membrane translocation. Mutig K, **Saritas T**, Uchida S, Kahl T, Borowski T, Paliege A, Böhlick A, Bleich M, Shan Q, Bachmann S. Am J Physiol Renal Physiol 2010;298(3):F500-1.

Tamm-Horsfall glycoprotein (THGP) interacts with renal potassium channel ROMK2 and regulates its function. Renigunta A, Renigunta V, **Saritas T**, Decher N, Mutig K, Waldegger S. J Biol Chem. 2011;286(3):2224-35.

Activation of the bumetanide-sensitive Na+,K+,2CL cotransporter NKCC2 is facilitated by tamm-horsfall protein in a chloride-sensitive manner. Mutig* K, Kahl T*, **Saritas T**, Godes M, Persson P, Bates J, Raffi H, Rampoldi L, Uchida S, Hille C, Dosche C, Kumar S, Castañeda-Bueno M, Gamba G, Bachmann S. J Biol Chem 2011;286(34):30200-10.

A SPAK isoform switch modulates renal salt transport and blood pressure. McCormick JA*, Mutig K*, Nelson JH***, Saritas T**, Hoorn EJ, Yang CL, Rogers S, Curry J, Delpire E, Bachmann S, Ellison DH. Cell Metab. 2011;14(3):352-64.

SPAK differentially mediates vasopressin effects on sodium cotransporters. **Saritas T**, Borschewski A, McCormick JA, Paliege A, Dathe C, Uchida S, Terker A, Himmerkus N, Bleich M, Demaretz S, Laghmani K, Delpire E, Ellison DH, Bachmann S, Mutig K. J Am Soc Nephrol. 2013;24(3):407-18.

Case Report: Akutes Nierenversagen, Verwirrtheit und Petechien nach Infekt in Ägypten. **Saritas T.** Der Nephrologe-Bild und Fall. Mai 2013.

Tari Z*, **Saritas T***, Blum C*, Gleim J*, Weller M*. Demografie als Herausforderung. WeltTrends: Zeitschrift für internationale Politik. Nr. 78. Mai/Juni 2011. ISBN: 978-3-941880-22-1.

Aktive Kongressbeiträge:

03/2009: Poster: 104th International Meeting of the Anatomische Gesellschaft, Antwerpen, Belgien.

10/2009: Vortrag: 20th European Student Conference, Berlin.

03/2010: Vortrag: 29th Annual Meeting of the West Coast Salt & Water Club, San Luis Obispo, Kalifornien, USA.

09/2010: Poster: 27. Arbeitstagung der Anatomischen Gesellschaft, Würzburg.

11/2010: Poster: 43rd Annual Meeting of the American Society of Nephrology ASN, Denver, Colorado, USA

04/2011: Vortrag and Poster: Pre-Experimental Biology and EB 2011, Washington DC, USA

05/2011: Vortrag: Joint Meeting of Anatomical Societies, Bursa, Türkei

09/2011: Poster: Jahrestagung der Deutschen Gesellschaft für Nephrologie, Berlin

11/2011: Poster: Concluding Symposium of the DFG-Research Unit FOR 667 Epithelial Mechanisms in Renal Volume Regulation, Berlin

03/2012: Vortrag: Annual Meeting of the Anatomische Gesellschaft 2012, Frankfurt.

10/2012: Vortrag: Jahrestagung der Deutsche Gesellschaft für Nephrologie, Hamburg.

6. Eidesstattliche Versicherung

„Ich, Turgay Saritas, versichere an Eides statt durch meine eigenhändige Unterschrift, dass ich die vorgelegte Dissertation mit dem Thema: [Kinase pathways involved in the vasopressin signaling along the distal nephron: roles of SPAK and OSR1 kinases] selbstständig und ohne nicht offengelegte Hilfe Dritter verfasst und keine anderen als die angegebenen Quellen und Hilfsmittel genutzt habe.
Alle Stellen, die wörtlich oder dem Sinne nach auf Publikationen oder Vorträgen anderer Autoren beruhen, sind als solche in korrekter Zitierung (siehe „Uniform Requirements for Manuscripts (URM)“ des ICMJE -*www.**icmje**.org*) kenntlich gemacht. Die Abschnitte zu Methodik (insbesondere praktische Arbeiten, Laborbestimmungen, statistische Aufarbeitung) und Resultaten (insbesondere Abbildungen, Graphiken und Tabellen) entsprechen den URM (s.o) und werden von mir verantwortet.
Meine Anteile an etwaigen Publikationen zu dieser Dissertation entsprechen denen, die in der untenstehenden gemeinsamen Erklärung mit dem/der Betreuer/in, angegeben sind. Sämtliche Publikationen, die aus dieser Dissertation hervorgegangen sind und bei denen ich Autor bin, entsprechen den URM (s.o) und werden von mir verantwortet.

Die Bedeutung dieser eidesstattlichen Versicherung und die strafrechtlichen Folgen einer unwahren eidesstattlichen Versicherung (§156,161 des Strafgesetzbuches) sind mir bekannt und bewusst.“

Datum Unterschrift

Anteilserklärung an etwaigen erfolgten Publikationen

Turgay Saritas hatte folgenden Anteil an den folgenden Publikationen:

Publikation 1: [Mutig K, **Saritas T**, Uchida S, Kahl T, Borowski T, Paliege A, Böhlick A, Bleich M, Shan Q, Bachmann S.], [Short-term stimulation of the thiazide-sensitive Na+,Cl cotransporter by vasopressin involves phosphorylation and membrane translocation.], [Am J Physiol Renal Physiol], [2010]
Beitrag im Einzelnen (bitte kurz ausführen): Figure 1-3, 5, S1 und S2: Immunhistochemische Färbung und konfokale Auswertung, Auswertung der Immunogold- Markierungen, Durchführung und Auswertung von Western blots.

Publikation 2: [Renigunta A, Renigunta V, **Saritas T**, Decher N, Mutig K, Waldegger S], [Tamm-Horsfall glycoprotein (THGP) interacts with renal potassium channel ROMK2 and regulates its function.], [J Biol Chem.], [2011]
Beitrag im Einzelnen (bitte kurz ausführen): Figure 1b: Immunhistochemische Färbung; Figure 6: Immunhistochemische Färbung, Durchführung und Auswertung von Western blots; Figure S3: Immunhistochemische Färbung.

Publikation 3: [Mutig* K, Kahl T*, **Saritas T**, Godes M, Persson P, Bates J, Raffi H, Rampoldi L, Uchida S, Hille C, Dosche C, Kumar S, Castañeda-Bueno M, Gamba G,

Bachmann S.], [Activation of the bumetanide-sensitive Na+,K+,2CL cotransporter NKCC2 is facilitated by tamm-horsfall protein in a chloride-sensitive manner.], [J Biol Chem], [2011]
Beitrag im Einzelnen (bitte kurz ausführen): Figure 2, 7, 8: Durchführung von Western blots. Figure 3: Zellkultur: Transfektion, immunhistochemische Färbung, Auswertung.

Publikation 4: [McCormick JA*, Mutig K*, Nelson JH***, Saritas T**, Hoorn EJ, Yang CL, Rogers S, Curry J, Delpire E, Bachmann S, Ellison DH.], [A SPAK isoform switch modulates renal salt transport and blood pressure.], [Cell Metab], [2011]
Beitrag im Einzelnen (bitte kurz ausführen): Figure 2: Immunhistochemische Färbungen, Durchführung von Western blots. Figure 4 A-D: Immunhistochemische Färbungen, Durchführung und Auswertung von Western blots. Figure 5 A-C, E-F: Immunhistochemische Färbungen, Auswertung der Immunogold-Markierungen. Figure 6 A-B: Immunhistochemische Färbungen.

Publikation 5: [**Saritas T**, Borschewski A, McCormick JA, Paliege A, Dathe C, Uchida S, Terker A, Himmerkus N, Bleich M, Demaretz S, Laghmani K, Delpire E, Ellison DH, Bachmann S, Mutig K.], [SPAK differentially mediates vasopressin effects on sodium cotransporters.], [J Am Soc Nephrol.], [2013]
Beitrag im Einzelnen (bitte kurz ausführen): Manuskripterstellung, Figure 1-3: Immunhistochemische Färbungen, konfokale Auswertung, Figure 5: Auswertung der Immunogold-Markierungen, Figure 4, 6, 9, 10: Durchführung und Auswertung von Western blots; Figure 7 C, D: Auswertung von Co-IP Versuchen; Figure 7 E, F: Durchführung und Auswertung von Western blots, Figure 11: Erstellung der Abbildung. S1-4: Durchführung und Auswertung von Western blots, Immunhistochemische Färbungen, PCR.

Unterschrift, Datum und Stempel des betreuenden Hochschullehrers/der betreuenden Hochschullehrerin

Unterschrift des Doktoranden/der Doktorandin

7. Lebenslauf

„Mein Lebenslauf wird aus datenschutzrechtlichen Gründen in der elektronischen Version meiner Arbeit nicht veröffentlicht.“